The Effects of Viscous Stresses and Mantle Velocities on Subduction; Finite Difference Modeling

by

Matthew Walter Dawson

Submitted to the Department of Earth, Atmospheric, and Planetary Sciences
in partial fulfillment of the requirements for the degree of

Master of Science in Earth and Planetary Sciences

at the

MASSACHUSETTS INSTITUTE OF TECHNOLOGY

September 2001

Author .....
Department of Earth, Atmospheric, and Planetary Sciences
June 12, 2001

Certified by .....
Leigh H. Royden
Professor
Thesis Supervisor

Accepted by .....
Ronald Prinn
Head, Department of Earth, Atmospheric, and Planetary Sciences

The Effects of Viscous Stresses and Mantle Velocities on Subduction; Finite Difference Modeling

by

Matthew Walter Dawson

Submitted to the Department of Earth, Atmospheric, and Planetary Sciences
on June 12, 2001, in partial fulfillment of the
requirements for the degree of
Master of Science in Earth and Planetary Sciences

Abstract

This thesis presents a two-dimensional finite-difference model of subduction, which is used to explore the characteristics of subduction that are most closely related to deformation in the overriding plate. The model focuses on how the angle, α, at which the slab subducts and the rate, v_r , at which the subduction boundary "retreats" are affected by the negative buoyancy of the subducting lithospheric slab and the viscous forces that arise where the mantle and subducting slab are in motion relative to one another.

The viscous forces acting on the slab are approximated as the product of the viscosity, $\mu = 10^{21} Pa \cdot s$, and the relative velocity of the subducting lithosphere and the surrounding mantle, divided by γ, the length-scale over which these viscous forces might operate. The model treats the normal and shear viscous forces seperately; the normal viscous force is equal to the slab-perpendicular component of the relative velocity times $\frac{\mu}{\gamma_N}$, whereas the shear viscous force equals the slab-parallel velocity component of the relative velocity times $\frac{\mu}{\gamma_S}$. When either γ_N or $\gamma_S = \infty$, the respective viscous force equals zero. If $\gamma_N = \gamma_S$, the direction of the net viscous force acting on the slab is parallel to the total velocity of the mantle relative to the slab. Problems with numerical stability in the *FORTRAN 90* code used to implement the model precluded the use of $\gamma_N = \gamma_S$; the largest stable $\frac{\gamma_N}{\gamma_S}$ ratio was $\frac{\gamma_N = 20km}{\gamma_S = 50km}$. These numerical instabilities could not be eliminated within the time constraints of this thesis.

I examine subduction into a mantle that moves horizontally at a velocity v_m. The velocity of the mantle, v_m, and the rate of retreat, v_r, are measured relative to a point on the subducting lithosphere far from the subduction boundary; in both cases, positive velocities are directed from the "back-arc" region toward the trench.

With a stationary mantle, ($v_m = 0$), $\gamma_S = \infty$ and $\gamma_N = 20$ km, the rate of subduction zone retreat, v_r, is ~ 101 mm/yr. The retreat rate varies linearly with γ_N, reaching 230 mm/yr when $\gamma_N = 45$ km. However, the subduction angle, α, remains approximately constant at $\sim 24°$. When γ_S is reduced from ∞ to 50 km, v_r slows to ~ 94 mm/yr and α increases to $\sim 26°$.

When the mantle moves at a rate v_m, with $\gamma_N = 20$ km (which is used for all cases where $v_m > 0$), and $\gamma_S = \infty$, v_r varies linearly with v_m, reaching ~ 148 mm/yr when $v_m = 50$ mm/yr. Under these conditions, the retreat rate is approximately equal to the velocity of the mantle plus the retreat rate in the absence of mantle motion. The subduction angle, α, remains near $\sim 24°$, only decreasing by $\sim \frac{1}{10}°$. When γ_S is reduced from ∞ to 200 km, v_r varies non-linearly with v_m, starting at ~ 99 mm/yr when $v_m = 0$ mm/yr and reaching ~ 132 mm/yr when $v_m = 50$ mm/yr. When γ_S is reduced further to 50 km, v_r actually *decreases* with increasing v_m, starting at ~ 94 mm/yr when $v_m = 0$ mm/yr and reaching ~ 89 mm/yr when $v_m = 50$ mm/yr. For both $\gamma_S = 200$ km and $\gamma_S = 50$ km, α increases with increasing v_m. When $v_m = 50$ mm/yr , $\gamma_S = 200$ km yields $\alpha = \sim 28°$ and $\gamma_S = 50$ km yields $\alpha = \sim 41°$. We suspect that smaller values of γ_S would have produced even steeper subduction angles had numerical difficulties not precluded our analysis of these conditions.

These results illustrate three main points: 1) Subduction angle and retreat rate *are* dependent on the viscous forces exerted upon the slab by the mantle, particularly on the ratio of the viscous forces that act perpendicular and parallel to the subducting slab. 2) The normal (slab-perpendicular) and shear (slab-parallel) viscous forces differ in their influences on subduction angle and retreat rate. 3) When slab-parallel viscous forces are small relative to the slab-perpendicular viscous forces, the angle of subduction is always shallow, near $\sim 25°$. 4) Steeply dipping subduction zones occur only when the slab parallel viscous forces are large and the mantle moves at a significant velocity relative to the subducting slab.

Future work with this model will examine how the density structure of the down-going lithospheric slab affects subduction and how its effects combine with those caused by the mantle-induced viscous forces.

Thesis Supervisor: Leigh H. Royden
Title: Professor

Acknowledgments

This thesis reflects not only the effort spent writing (and editing) text and drawing figures for the past few weeks; it represents the culmination of six years of study in the earth sciences, which started at one Tech and ended up at another.

Therefore, before I run off to submit this work, I would like to take a minute to thank a few people who helped me make it this far.

I'll start with the entire 8th Floor, since they helped me with pretty much everything since I arrived at MIT. From advising me about the classes to take or avoid, to helping me with problem sets, to loaning me books and papers, to always directing me toward the free food– they helped me stay focused. Amy taught me *Canvas*, Bill taught me *LaTeX* , Steve reminded me to automate everything possible, John helped me through a number of computer issues, Roberta kept everything running smoothly, Marin and Fernanda were great office-mates, and Wiki was a great advisor who A) taught me about subduction, B) let me work through things when I needed to, and C) pointed me in the right direction when I got stuck. *"Efharisto poly!"*

I'd also like to thank my family and friends, at MIT, Caltech, and elsewhere, for encouraging me in my studies, my writing, and my pursuit to find "my thing." To Jennie, thank you for listening to all of my discussions of vectors and *FORTRAN*, and for proofreading and re-proofreading my writing.

And of course, thank you to MIT and Caltech for teaching me in six years more than I had expected to learn... ever.

Contents

List of Figures

Chapter 1

Introduction

1.1 Plate Tectonics

The theory of plate tectonics changed the way we look at the earth and revolutionized the field of geology. In the plate tectonic view, the earth's surface, or lithosphere, consists of a collection of stiff plates that float atop a softer layer, or asthenosphere. The approximately 100 kilometer thick lithosphere, whose name derives from the Greek word "lithos" (*rock*), includes the crust as well as the uppermost, stiff portion of the mantle. The asthenosphere, whose name derives from the Greek word "asthenia" (*weak*, or *sick*), comprises the viscous portion of the mantle that extends from a depth of about 100 kilometers to $\sim$ 350 kilometers [2]. The plates of the earth's lithosphere are in constant motion, sliding past one another at transform (conservative) boundaries, moving toward each other at convergent (destructive) boundaries, or spreading apart at divergent (constructive) boundaries.

1.2 Subduction and Slab-Pull

At mid-ocean ridges, new oceanic crust is generated along the boundary between diverging lithospheric plates. Globally, the birth of new crust along mid-ocean ridges is balanced by the consumption of old crust at subduction zones. A subduction zone arises when a slab of the earth's lithosphere, usually aging oceanic lithosphere,

develops a density greater than the underlying mantle and upsets isostatic balance. The densified, negatively buoyant slab sinks into the mantle, resulting in the process known as subduction, which is illustrated in Figure A-1. The mass of the subducted portion of the lithosphere transfers a downward force along the length of the slab, which progressively pulls more material into the mantle and creates a net convergence between the downgoing slab and the plate under which it dives. This downward force, known as the "slab-pull" force, is thought to play an important role in driving the overall movement of lithospheric plates. Consequently, the location and rate at which subduction occurs acts as a general constraint on the magnitude and direction of global plate motions. Therefore, a thorough knowledge of subduction processes is vital to our understanding of plate tectonics on a global scale.

Chapter 2

Motivation and Objective

2.1 "Narrow" Subduction Zones

Subduction zones, the linear regions where (typically oceanic) lithosphere is consumed are dispersed throughout the globe along convergent plate boundaries. Due to the flexural down-bending of the subducted plate, subduction zones are often marked by deep trenches, which represent the deepest reaches of the world's oceans. Sedimentary material scraped off the downgoing slab may comprise a synthetic fold-and-thrust belt located adjacent to the trench. Dewatering of the progressively heated subducted crust may enhance partial melting in the overriding slab, resulting in the production of a volcanic arc, which accompanies many subduction zones. Although many subduction zones share the above features, their characteristics vary from place to place depending on a variety of factors, such as the *rate* at which the subducting plate is consumed, the *angle* between the subducting plate and the surface, and the *depth* to which the subducted plate extends [2].

Another factor affecting subduction is the *width* of the subduction zone. In this paper, we speak of width in terms of the lateral distance covered by a subduction boundary in map-view. Wider subduction zones have a greater potential impact on global plate motions, but their size renders them more difficult to model then narrower, less extensive subduction zones. This difficulty arises from the obscured influence large sections of subducted lithospheric slabs may have on patterns of mantle

motion and convection, which in turn influence the subduction process in a complicated feedback loop. On the other hand, narrower, more localized subduction zones may not have a very large influence on global mantle flow patterns or global plate motions. Thus, while the behavior of narrow subduction zones is subject to the boundary conditions imposed by motion on major plate boundaries and by major, global convection patterns in the asthenosphere, their motions are largely controlled by the more localized slab-pull force. The slab-pull force is determined by the variables that affect the downgoing slab in the vicinity of the subduction zone. These variables include the density structure of the downgoing slab, the density structure of the overriding plate, small scale variations in geometry, and perhaps localized, small scale mantle motions. Consequently, short subduction zones that have locally determined boundary conditions and evolve independently of far-field influences can be analyzed and modeled more directly and straightforwardly than their longer counterparts.

While short subduction zones may not appear important on a global scale, they are often very important in determining the nature of local oceanic and continental tectonics. For instance, the thoroughly studied Alps consist of sets of stacked nappes which were thrust atop one another as subduction along short convergent zones brought portions of buoyant continental or island arc crust into contact. Likewise, the formation of basins behind the volcanic arc, or in the "back-arc" region, observed at locations in the West Pacific Ocean and the Aegean Sea, is caused by the retreat of short subduction boundaries. Thus, an understanding of short subduction zones can provide insight about a wide range of tectonic styles and regimes.

2.2 Subduction Zone "Retreat" and Back-arc Basins

Of specific interest to us is the relationship between subduction zone "retreat" and back-arc extension. A subduction boundary may retreat, or migrate away from the overriding plate (toward the foreland) when the downgoing plate descends at a rate that exceeds the rate of convergence between the stable portions of the two involved plates. As the subduction boundary migrates back toward the foreland faster than the

overriding plate converges, compressive stress against the overriding plate is reduced. This allows the overriding plate, which while converging, would normally be in a state of compression, to actually extend, effectively "filling the gap" that otherwise would result from the disparity between subduction and convergence rates [5, 4, 3]. The result is a "back-arc basin," which, as its name might suggest, usually occurs on the "back" side of the volcanic arc, opposite the subduction zone. Some back-arc basins may form partially coincident with a current or older arc, thus dissecting them and obscuring their signature in the geologic record.

Many back-arc basins contribute to the formation of marginal seas, which appear intact in the West Pacific and behind Alaska's Aleutian Islands, and are found as ophiolitic slivers in the Alps. Other back-arc basins have been identified near the Carpathians and in the Aegean region [6, 4, 3]. Thus, the phenomenon of back-arc spreading is widespread, and careful geologic mapping and plate reconstructions have shown that it is a transitory process that has the ability to migrate quickly and to turn on and off over short periods of time.

The tectonic state of back-arc regions may oscillate from extensive, where the locally subducting slab was probably in a state of retreat (Carpathian), to neutral, where the local subduction and convergence rates are approximately in balance (Sumatran), to compressive, where the rate of convergence may have overtaken the rate of subduction (Andean). To understand how these changes occur, we should understand what factors might control subduction rates.

The rate of subduction, however, is not alone in its effects on the tectonics of the overriding plate. The angle at which one plate dives beneath another might also have important consequences, as is believed to be the case along the western margin of South America. As the Andes Mountains have grown from a combination of compression and arc volcanism, there might be an additional contribution related to the effective crustal thickening that might result from the "underplating" of the subducting slab on to the overriding plate. Isostatic balance would lead the thickened crust to "float" high on the mantle. The interesting range of possible cause-and-effect relationships between the characteristics of subduction and upper-plate deformation

allows us to use our modeling efforts to learn more about back-arc extension.

A better understanding of the behavior of back-arc basins would increase our knowledge of the past, present, and future of the regions in which they appear, such as the Aegean. In this thesis, we attempt to attain a better understanding through the development and analysis of a general model of narrow subduction zones. The model attempts to describe the evolution and the initiation of the types of subduction zones in which slab-pull might dominate over far field stresses and create the conditions necessary for back-arc spreading. Specifically, we aim to learn what factors might cause subduction rates to slow down or speed up. We also hope to gain insight regarding the variables that might control the angle at which a slab descends and the geometry it assumes. One obvious input is the density structure of the downgoing slab. We examine slabs of low, high, and spatially varying densities to see how the spatial and temporal evolution of short subduction zones might be affected. Local motions of the mantle will also be considered. We will examine cases where the asthenosphere is stationary and compare those results to those obtained when the asthenosphere is assigned a simple motion. It will be important to note both the length and time scales over which the effects of density variations or mantle motions can be detected. Of particular interest will be the implications for their control on the actual three (or four) dimensional geometry and evolution of short subduction zones.

Chapter 3

Method

3.1 Intent of Model

The model presented in this paper is not intended to recreate any specific subduction zone from the past or present. Instead, our aim is to utilize a model to explore the *processes* that might be common to a variety of subduction zones, particularly narrow ones. Our focus on short subduction zones, like those found in the Aegean and along segments of the West Pacific subduction boundaries, allows us to set aside the influence of global lithospheric plate motions and global asthenospheric convection currents. Although these large scale and far-field forces can never completely be discounted, we hope that a concentration on forces more local to the subduction zone might yield important insights about general subduction behavior, especially for zones that lack great width. The following section summarizes the physical processes considered in our numerical model of subduction.

3.2 The Flexure Equation

The fundamental assumption of plate tectonics is that the lithosphere is a collection of stiff, relatively thin plates that "float" on top of the asthenosphere, which includes the weakest portion of the mantle [2]. The plates of the lithosphere are generally taken to behave rigidly within their interiors, with large-scale deformation concen-

trated along plate boundaries. On a geologic time scale, which is the concern of this study, the deforming lithosphere behaves as an elastic solid [2]. Like any other elastic material, the elastic behavior of the lithosphere can be characterized by two material parameters: Young's Modulus (E) and Poisson's Ratio (ν) [7]. In contrast to the lithosphere, the asthenosphere, as its name might suggest, behaves as a viscous fluid on a geologic time scale. Thus, the way in which the asthenosphere, as well as the rest of the mantle (at least down to $\sim$ 600 km), responds, or strains, under an applied stress can be characterized by the parameter known as viscosity (μ) [7]. These descriptions of the lithosphere and mantle serve as the starting point for most models of subduction, including the one presented in this study.

The study of continuum mechanics, a staple of engineering, materials science, and of course, geodynamics, provides us with a differential equation to describe the vertical deflection (w) of a thin elastic plate as a function of horizontal distance (x). This equation, known as the "flexure" equation, takes the form:

$$D\frac{d^4w}{dx^4} = V(x) - H\frac{d^2w}{dx^2} \tag{3.1}$$

In the flexure equation, V represents the vertical force per unit length, or vertical stress, applied to the plate as a function of horizontal distance (x). The term H represents a horizontal compressive stress applied along the length of the plate. The constant D is known as the lithosphere's *flexural rigidity*, or elastic strength. Flexural rigidity depends on the elastic parameters E and ν, as well as the lithosphere's effective elastic thickness (h) through the relation

$$D = \frac{Eh^3}{12(1-\nu^2)} \tag{3.2}$$

For our model of subduction, we use the same general form as the above flexure equation, but with a few simple adjustments. In order for it to be more easily solved by analysis, the form of the flexure equation shown in Equation 3.1 is derived for a deflection (w) sufficiently small that the "small angle approximation" may be used to equate the plate's slope ($\frac{-dw}{dx}$) to its angular deflection (α). The assumption of a small

deflection seems reasonable, since under most conditions, the lithosphere's strength is sufficient to prevent it from bending at large angles. In our model, however, we wish to examine a full range of plate geometries and angles of deflection. To accomplish this, we omit the small deflection assumption and instead derive a form of the flexure equation that can accommodate a deflection of any magnitude at any angle, so long as the resulting geometry is physically feasible. We also make a slight adjustment in flexure equation's reference frame. The typical flexure equation relates vertical deflection (w) to horizontal distance (x), which is most convenient because it mirrors what we can actually observe at the earth's surface. However, since our model of subduction will be solved numerically, at nodes equally spaced along the subducting plate, we derive the flexure equation in the reference frame of distance along the plate, along a coordinate we will call s.

3.3 Forces

Although our derivation, which will be shown in full later, makes slight adjustments to the flexure equation, the forces acting upon the subducting plate are fundamentally the same. The only body force exerted on the plate is the force of gravity. The graviational force is directed downward and is proportional to the plate's mass, which is equal to the product of its thickness (h) and density (ρ). All other forces considered in our model act directly on the upper and lower surfaces of the subducting plate. These forces can be divided into two main categories: pressure forces and viscous forces, which in turn can each be divided into two sub-categories.

3.3.1 Pressure Forces

All pressure forces, by definition, are exerted normally (perpendicularly) to the plate's surface. The two types of pressure forces are those exerted on the upper surface of the plate and those exerted on the lower surface. The pressure exerted at a point on the upper surface of the plate is due to the combined mass of all the material positioned in a column directly above that point. As shown in Figure A-2 the material pressing

down on a point on the upper surface may include a combination of asthenospheric mantle, lithospheric mantle, lithospheric crust (continental or oceanic), or water, depending on the positioning of that point relative to the overriding plate. For example, the downward pressure exerted on the subducting slab at position (A) in Figure A-2 would amount to

$$P_{(A)} = \rho_c g h_c + \rho_m g h_m + \rho_a g h_{a1} \tag{3.3}$$

The pressure exerted at a point on the lower surface of the subducting plate may be thought of as a *restoring* force that results from the displacement of dense mantle by the sinking lithospheric slab. As the plate subducts, its lower density mass displaces the higher density mass of the mantle. This displacement upsets isostatic balance, so a net pressure, or restoring force, is exerted to the underside of the plate.

3.3.2 Viscous Forces

Viscous forces are applied to the subducting, elastic lithosphere where it is in motion relative to the surrounding, viscous mantle. While stress in an elastic medium is proportional to strain, in a viscous medium like the mantle, stress is related to strain *rate*, which is equivalent to velocity gradient. In a *Newtonian* fluid, stress (σ) is linearly proportional to strain rate ($\dot{\varepsilon}$)

$$\sigma = \mu \dot{\varepsilon} \tag{3.4}$$

where μ, the constant of proportionality, is considered the *viscosity* [7]. Both the viscosity and the function that relate stress to strain rate in a fluid depend on the specific characteristics of that fluid. For instance, in some Newtonian fluids, such as those whose mode of deformation is dominated by diffusion creep, viscosity is directly proportional to the exponential of the inverse absolute temperature of the fluid. In fluids whose mode of deformation is dominated by dislocation creep, not only is viscosity temperature dependent, but strain rate and stress are related through a power-law. Fluids like these, in which stress and strain rate are not linearly related

are called *non-Newtonian* fluids [7].

Experimental studies show that the high-temperature deformation of olivine, the chief mineral constituent of the mantle, corresponds well to a power-law rheology in which strain rate is proportional to the cube of stress. However, studies of bulk mantle viscosity, like those utilizing glacial rebound, have a difficult time discriminating between Newtonian and non-Newtonian rheologies. This difficulty might be due to viscosity's dependence on temperature, which is common to both diffusion and dislocation creep and appears to exert more control on overall mantle rheology than does viscosity's dependence on stress [7]. In our model, due to the lack of definitive evidence for the stress dependence of the mantle's viscosity and in order to unravel the basic connections between viscous resistance along a subducting slab and the resulting subduction rates and geometries, we consider the mantle to behave approximately as a Newtonian fluid, with a viscosity $\mu = 10^{21} Pa \cdot s$. We take the viscous force, σ_{visc} , to be linearly proportional to velocity gradient, which we approximate as the relative velocity, v_{rel} , between the subducting slab and the surrounding mantle. Thus, we can write the viscous force as

$$\sigma_{visc} = v_{rel} \frac{\mu}{\gamma} \tag{3.5}$$

where μ is the mantle viscosity and γ is the length scale over which the viscous forces might act. To illuminate the way in which the viscous force applied by the mantle to the lithosphere affects subduction angle and retreat rate, we deconstruct the viscous force into two components: the normal and shear (tangential) viscous forces. The normal and shear viscous forces are examined individually and are given by

$$\sigma_{visc,N} = v_{rel,\perp} \frac{\mu}{\gamma_N} \quad and \quad \sigma_{visc,S} = v_{rel,\parallel} \frac{\mu}{\gamma_S} \tag{3.6}$$

where $v_{rel,\perp}$ and $v_{rel,\parallel}$ are the slab-perpendicular and slab-parallel components of the total vector representing the relative velocity between the subducting slab and the surrounding lithosphere. Note that each viscous force has its own γ as well, which

is used to compare and contrast the effects of the two viscous forces on subduction angle and retreat rate. To remove one of the viscous forces from our model, we set its $\gamma = \infty$. For similar viscous forces, we would use $\gamma_N = \gamma_S$. However, the *FORTRAN 90* code used to run the model (as described in the following chapter) could not produce stable numerical results for $\gamma_N = \gamma_S$; the closest the ratio $\frac{\gamma_N}{\gamma_S}$ could approach unity while maintaining numerically stable results was $\frac{\gamma_N = 20km}{\gamma_S = 50km}$.

Our model initially consists of an elastic plate subducting from right to left through a stationary, viscous mantle. As the plate moves through the mantle, the mantle opposes the motion with a viscous resistance force directed against the direction of motion and exerted upon one or both of the plate's surfaces, depending on the relative velocity vectors of the mantle and lithospheric plate. The resistance of the mantle against the free end of the subducting plate has not been considered yet, but future work with this model will probably include that additional factor.

While the mantle's resistance to a falling or retreating lithospheric plate provides the first source of viscous force, the second type of viscous force arises when the mantle is no longer stationary, but instead has some initial motion relative to the lithosphere, aside from any relative motion due to the action of subduction. Since our model of narrow subduction zones will not incorporate global, large-scale convection currents, we model local mantle motions in a very simple, straightforward manner; the mantle moves either toward the right, incident upon the top of the subducting slab, or toward the left, incident upon the bottom of the subducting slab. In either case, the mantle moves parallel to the earth's surface with a uniform velocity, v_m, so there is no velocity gradient within the mantle. This additional relative motion of the mantle against the lithosphere applies another viscous force to the subducting slab that will either counter or enhance the viscous resistance force described earlier.

Chapter 4

Derivation of Flexure Equation

This section outlines the assumptions made and the steps taken to derive the flexure equation used in our model. The assumptions are based on the physical model described above, and the derivation process roughly parallels the traditional derivation, as given in Turcotte and Schubert's text, *Geodynamics* [7].

One of the distinguishing characteristics of our derivation is the coordinate system. Our desired result is a differential equation that relates deflection to position along the plate. To achieve this, we use the coordinate system illustrated in Figure A-3, where z is the vertical coordinate and s measures position along the subducting plate. Deflection, w, is measured vertically along the z-axis and is considered to be zero at sea level, increasing positively downward. Position, s, is taken to be zero at the subducting plate's free end and increases positively to the right, toward the plate's interior. The s-axis runs through the middle of the lithosphere, splitting it into an upper and lower half. The y-axis is perpendicular to the s-axis and measures the thickness of the lithosphere. The y-coordinate is zero along the s-axis, positive in the upper half of the lithosphere, and negative in the lower half. The primary horizontal coordinate, x, starts at zero at the extreme left of Figure A-3 and also increases positively toward the right. For all points along the lithosphere with zero deflection, $x = s$. Although the x-coordinate is not used directly in our derivation, it will be discussed later in relation to our model's results. The secondary horizontal coordinate, b , lies along an axis perpendicular to both the x and z-axes. The positive

b-axis points "into" the plane of Figure A-3. The angle of deflection, at any position along the plate, will be referred to as α.

Having established the coordinate system, we can begin to derive the flexure equation. Our flexure equation, like any other, is based on the idea that the flexing lithosphere must be in a state of equilibrium. By analyzing the balance of forces and torques exerted upon the lithosphere, we can determine the resulting deflection [7]. To conduct this analysis, we focus on a small element of lithospheric plate, with length ds, and examine the forces and torques that act upon the element. The element of lithosphere and all acting forces and torques are illustrated in Figure A-4. Note that the segment extends from position (s) to position $(s+ds)$, and the angle of deflection increases from (α) at position (s) to $(\alpha + d\alpha)$ at position $(s + ds)$.

The sum of all the pressure and viscous stresses applied to the lithosphere's surface results in both a net vertical stress, q_v, and a net horizontal stress, q_h, which are defined as positive in concert with the directions of increasing deflection (w) and increasing horizontal distance (x) respectively. The total force, per unit length along the b-axis, exerted by q_v on the segment of lithosphere is $q_v ds$, and the total force exerted by q_h is $q_h ds$. Any lithospheric cross section, with a surface perpendicular to the s-axis, will experience a collection of shear stresses. The integration of all these shear stresses over the area spanned by the cross section results in a net shear force, per unit length along the b-axis. The net shear force acting along a cross section at position (s) is (V), while the net shear force acting along a cross section at position $(s+ds)$ is $(V+dV)$. The respective directions of these net shear forces are illustrated in Figure A-4.

An additional force, per unit length along the b-axis, might be applied to the ends of a lithospheric segment, directed along the s-axis. This force has magnitude (C) at position (s) and $(C+dC)$ at position $(s+ds)$, with directions illustrated in Figure A-4. The force we call C in this study is somewhat analagous to the horizontal force given by P in Turcotte and Schubert's text [7]; the difference is that C is dependent on the position along the plate (s), whereas P is held constant, independent of horizontal position (x). In addition to the net forces described above, a net *bending moment* (M)

also acts on each cross section of the flexing lithosphere. As a segment of lithosphere is flexed as shown in Figure A-4, lengthwise contraction occurs in the upper half and lengthwise extension occurs in the lower half. The contraction within the upper half is accompanied by negative stress and strain, whereas the extension in the lower half is accompanied by positive stress and strain. The stresses, when multiplied by y, their distance from the central s-axis, and then integrated over a lithospheric cross section with thickness h, yields the net bending moment. The relationship between the net bending moment (M) and the longitudinal strain (ε_{ss}) caused by flexure is

$$M = \frac{E}{(1-\nu^2)} \int_{\frac{-h}{2}}^{\frac{h}{2}} \varepsilon_{ss} y dy \tag{4.1}$$

where (E) is Young's Modulus and (ν) is Poisson's ratio.

This equation will be used shortly to relate the forces exerted upon the lithosphere to its deflection. For details regarding the relationship between the net bending moment (M) and the longitudinal strain (ε_{ss}), refer to Turcotte and Schubert's text. The net bending moment has magnitude (M) at position (s) and magnitude ($M+dM$) at position ($s+ds$). The directions of the bending moment are illustrated in Figure A-4. Now that we have described the forces and torques applied to an element of flexing lithosphere, we may begin to examine the implications of the equilibrium requirement. A balance , or zero sum, of all vertical components of force yields

$$0 = V_{vert,total} + C_{vert,total} + q_{vert}(s)ds \tag{4.2}$$

$$0 = -V\cos\alpha|_s + V\cos\alpha|_{s+ds} - C\sin\alpha|_s + C\sin\alpha|_{s+ds} + q_v(s)ds \tag{4.3}$$

Taking the limit as $ds \longrightarrow 0$, the above expression produces the differential equation

$$0 = \frac{d}{ds}(V\cos\alpha) + \frac{d}{ds}(C\sin\alpha) + q_v(s) \tag{4.4}$$

or:

$$K_v = V\cos\alpha + C\sin\alpha + \int_0^s q_v(s)ds \tag{4.5}$$

where K_v is an arbitrary constant and $\int_0^s q_v(s)ds$ represents the integral, taken from the end of the plate (where $s = 0$) to the position s, of all forces applied vertically to the surfaces of the lithosphere. Note that at the free end of a subducting slab, where $s = 0$,

$$V = C = 0 \longrightarrow K_v = 0 \tag{4.6}$$

Mirroring the above process, a balance of all horizontal force components yields

$$0 = -V_{horiz,total} + C_{horiz,total} + q_{horiz}(s)ds \tag{4.7}$$

$$0 = -V\sin\alpha|_s + V\sin\alpha|_{s+ds} + C\cos\alpha|_s - C\cos\alpha|_{s+ds} + q_h(s)ds \tag{4.8}$$

In the limit as $ds \longrightarrow 0$, the above expression produces the differential equation

$$0 = \frac{d}{ds}(V\sin\alpha) - \frac{d}{ds}(C\cos\alpha) + q_h(s) \tag{4.9}$$

or:

$$K_h = V\sin\alpha - C\cos\alpha + \int_0^s q_h(s)ds \tag{4.10}$$

where K_h is an arbitrary constant and $\int_0^s q_h(s)ds$ represents the sum, taken from the end of the plate (where $s = 0$) to the position s, of all forces applied horizontally to the surfaces of the lithosphere. Again note that at the free end of a subducting slab

$$V = C = 0 \longrightarrow K_h = 0 \tag{4.11}$$

We must also balance all torques applied to the element of lithosphere. Since the forces (C) and $(C + dC)$ act directly opposite one another along the s-axis, they

contribute no torque. The forces (V) and $(V + dV)$ both act in directions normal to the s-axis and therefore contribute quantities of torque equal to the products of their magnitudes and distances from the center of the element being balanced. The bending moments (M) and $(M + dM)$ are also torques. Thus, if we define positive torque as acting in the counterclockwise direction, a balance of the torques yields

$$0 = (M + dM) - (M) - (V + dV)\frac{ds}{2} - (V)\frac{ds}{2} \tag{4.12}$$

which can be simplified to

$$V + \left(\frac{1}{2}\right) dV = \frac{dM}{ds} \quad , \quad where \quad \left(\frac{1}{2}\right) dV \longrightarrow 0 \tag{4.13}$$

Since the torque $(dVds)$ produced by the term dV in the above equation becomes vanishingly small, we can eliminate the term $\left(\frac{1}{2}\right)) dV$, which leaves us with

$$V = \frac{dM}{ds} \tag{4.14}$$

This provides us with a direct relation between the net shear force (V) and the bending moment (M) that develops in response. As we have seen earlier, in Equation 4.1, the bending moment (M) is directly related to the strain (ε_{ss}) experienced by the lithosphere. Since the degree of strain ultimately determines the lithosphere's vertical deflection, we will use this series of connections to derive the relationship between the lithosphere's deflection and the forces that cause it. To understand exactly how longitudinal strain (ε_{ss}) relates to deflection (w) we must closely examine the geometry of the flexing lithosphere. As shown in Turcotte and Schubert [7],

$$\varepsilon_{ss} = \frac{-\Delta\ell}{\ell} = \frac{y}{R} \tag{4.15}$$

where ℓ is the length of the element along the s-axis, $\Delta\ell$ is the change in length along the s-axis, y is the distance from the s-axis, and R is the local radius of curvature of the lithosphere. Since we are deriving the equation for the s rather than the x coordinate system, we have replaced Turcotte and Schubert's ε_{xx} with ε_{ss}.

Turcotte and Schubert [7] also shows us that

$$R = \frac{\ell}{\phi} = \frac{\ell}{d\alpha} \tag{4.16}$$

where ϕ is the angle of curvature and $d\alpha$ is the change in angular deflection. If we substitute this expression for R into the above expression for ε_{ss} , we obtain

$$\varepsilon_{ss} = y\frac{d\alpha}{\ell} \tag{4.17}$$

In Turcotte and Schuberts derivation, angular deflection is taken to be very small, allowing the use of the small angle approximation to equate α to $\frac{-dw}{dx}$, or $\tan\alpha$. However, we do not place this restriction on α , and therefore, can not use the above approximation to relate ε_{ss} to deflection. Instead, our reliance on the s-coordinate rather than the x-coordinate provides us with the obvious but useful equality

$$\ell = ds \tag{4.18}$$

which allows us, by substitution of ds into Equation 4.17 to write

$$\varepsilon_{ss} = y\frac{d\alpha}{ds} \tag{4.19}$$

At this point, we have successfully related the longitudinal strain associated with the bending moment to the angle of deflection. However, our goal is to learn how the longitudinal strain relates to the actual deflection (w), which will allow us to ultimately determine the lithosphere's deflection when given a set of applied forces. Thus, our next step must be to connect the angle of deflection (α) to the actual deflection (w) . The connection between α and w is highlighted in Figure A-5, starting with

$$\sin\alpha = \frac{-dw}{ds} \equiv -w_s \tag{4.20}$$

where w_s is simply shorthand for $\frac{dw}{ds}$. The trigonometric identity $\sin^2\alpha + \cos^2\alpha = 1$ yields the expression

$$\cos\alpha = \sqrt{1-\sin^2\alpha} \equiv \sqrt{1-w_s^2} \tag{4.21}$$

Differentiation, with respect to s , of the above expression for $\sin\alpha$ leads us to an expression for $\frac{d\alpha}{ds}$ that includes w and is suitable for substitution into the above expression for ε_{ss}, Equation 4.19 .

$$\frac{d}{ds}(\sin\alpha) = \frac{d}{ds}\left[\frac{-dw}{ds}\right] \tag{4.22}$$

$$\frac{d\alpha}{ds}\cos\alpha = \frac{-d^2w}{ds^2} \equiv -w_{ss} \tag{4.23}$$

$$\frac{d\alpha}{ds} = \frac{-w_{ss}}{\sqrt{1-w_s^2}} \tag{4.24}$$

where w_{ss} is shorthand for $\frac{d^2w}{ds^2}$. Substitution of the above expression for $\frac{d\alpha}{ds}$ into 4.19 allows us to write

$$\varepsilon_{ss} = y\left[\frac{-w_{ss}}{\sqrt{1-w_s^2}}\right] \tag{4.25}$$

finally providing us with the direct relationship between longitudinal strain (ε_{ss}) and vertical deflection (w). This relationship can be entered into Equation 4.1, the earlier expression for bending moment (M) to give

$$M = \frac{E}{(1-\nu^2)}\int_{\frac{-h}{2}}^{\frac{h}{2}}\left[\frac{-w_{ss}}{\sqrt{1-w_s^2}}\right]y^2dy \tag{4.26}$$

Integration between $\frac{-h}{2}$ and $\frac{h}{2}$ yields

$$M = \frac{Eh^3}{12(1-\nu^2)}\left[\frac{-w_{ss}}{\sqrt{1-w_s^2}}\right] \tag{4.27}$$

where the quantity $\frac{Eh^3}{12(1-\nu^2)}$ is referred to as D, the flexural rigidity, or effective strength of the plate, giving

$$M = \frac{-Dw_{ss}}{\sqrt{1 - w_s^2}} \tag{4.28}$$

Now that we have successfully connected the bending moment (M) to the deflection (w) , we can further use this connection to relate w to the previously balanced vertical and horizontal force components. We begin by substituting our new expression for the bending moment into Equation 4.14, our earlier expression for net shear force, which yields

$$V = \frac{d}{ds}\left[\frac{-Dw_{ss}}{\sqrt{1 - w_s^2}}\right] \tag{4.29}$$

This expression, relating V to w , satisfies the condition of balanced torques. In order for it to be compatible with the other equilibrium conditions, we must insert it into some combination of the two equations describing the vertical and horizontal force balances. One combination, which conveniently eliminates the force C , can be obtained by multiplying Equation 4.5 by $\sqrt{1 - w_s^2}$ and adding that product to the product of Equation 4.10 and $-w_s$. The result of this combination is

$$K_v\sqrt{1 - w_s^2} - K_h w_s = V + \sqrt{1 - w_s^2}\int_0^s q_v ds - w_s \int_0^s q_h ds \tag{4.30}$$

which represents the addition of the components of the vertical and horizontal vorces that are normal to the subducting slab's surface. Substituting the expression for V given in Equation 4.29 into Equation 4.30 yields the differential equation

$$K_v\sqrt{1 - w_s^2} - K_h w_s = \frac{d}{ds}\left[\frac{-Dw_{ss}}{\sqrt{1 - w_s^2}}\right] + \sqrt{1 - w_s^2}\int_0^s q_v ds - w_s \int_0^s q_h ds \tag{4.31}$$

which can be differentiated with respect to s to give

$$-w_{ss}\left(\frac{K_v w_s}{\sqrt{1-w_s^2}}+K_h\right)=\frac{d^2}{ds^2}\left[\frac{-Dw_{ss}}{\sqrt{1-w_s^2}}\right]-\left[\frac{w_s w_{ss}}{\sqrt{1-w_s^2}}\right]\int_0^s q_v ds-w_{ss}\int_0^s q_h ds+q_v\sqrt{1-w_s^2}-q_h w_s \tag{4.32}$$

Rearranging and redistributing some of the terms of the above equation yields

$$\left[\frac{Dw_{ss}}{\sqrt{1-w_s^2}}\right]_{ss}+w_{ss}\left(\frac{w_s}{\sqrt{1-w_s^2}}\left[\int_0^s q_v ds-K_v\right]+\int_0^s q_h ds-K_h\right)-[q_n]=0 \tag{4.33}$$

where we have defined q_n , the net force applied normally to the subducting lithosphere, as

$$q_n=\left[q_v\sqrt{1-w_s^2}-q_h w_s\right] \tag{4.34}$$

We then use Equation 4.6 and Equation 4.11 to eliminate K_v and K_h from Equation 4.33 for a free slab end. The final differential equation describing the vertical deflection of a loaded lithospheric plate takes the form

$$\left[\frac{Dw_{ss}}{\sqrt{1-w_s^2}}\right]_{ss}+w_{ss}\left(\frac{w_s}{\sqrt{1-w_s^2}}\int_0^s q_v ds+\int_0^s q_h ds\right)-[q_n]=0 \tag{4.35}$$

or, when inserting Equation 4.34, the definition of q_n ,

$$\left[\frac{Dw_{ss}}{\sqrt{1-w_s^2}}\right]_{ss}+w_{ss}\left(\frac{w_s}{\sqrt{1-w_s^2}}\int_0^s q_v ds+\int_0^s q_h ds\right)-\left[q_v\sqrt{1-w_s^2}-q_h w_s\right]=0 \tag{4.36}$$

This fourth order differential equation serves as the basis for our model of subduction. We use numerical solutions of this equation under a variety of conditions to explore the factors that might affect the rate or angle of subduction at short subduction boundaries.

Chapter 5

Numerical Computation

5.1 Solving the Flexure Equation

The subduction of a plate of lithosphere is described by the flexure equation, which we derived in the previous chapter. The flexure equation relates the fourth and second derivatives of deflection w, with respect to position s, to the forces that act on the body and surface of the subducting plate. A solution to this differential equation would provide a functional relationship between between w and s, thus allowing us to specify the complete geometry of the subducting lithosphere. Since our flexure equation is actually a complicated combination of differentials and integrals, analytic solutions would be difficult, if not impossible, to obtain. To get around this difficulty, we use a finite difference approximation of the fourth and second order terms of the flexure equation to obtain numerical solutions. Additionally, by solving the flexure equation numerically, we can easily incorporate the time dimension into our model. This allows us to calculate both the subduction zone's spatial *and* temporal evolution, which are vital to our understanding of the relationships between the action of subduction and deformation within the overriding plate.

5.2 Finite difference approximation of flexure equation

To find numerical solutions to the differential equation shown in Equation 4.36, we use a computer program to solve the equation given by its *finite difference approximation.* The fourth and second order terms of the flexure equation can be approximated as *finite differences* by using the formal definition of the derivative. Given a function

$$y = f(x) \tag{5.1}$$

the first derivative, $\frac{dy}{dx}$, is defined as

$$\frac{dy}{dx} = \lim_{dx \to 0} \frac{f(x + dx) - f(x - dx)}{2dx} \tag{5.2}$$

If we consider equation 5.2 in the case where dx has a size that is finite but not approaching zero, we are left with the centered difference approximation for the first derivative

$$\frac{dy}{dx} \approx \frac{f(x + dx) - f(x - dx)}{2dx} \tag{5.3}$$

To approximate the second derivative, we perform the same calculation, but with the approximation of the first derivative substituted for $f(x)$. The third and fourth derivatives can be approximated in a similar fashion. The finite difference approximation of a differential equation containing terms of various orders is simply the sum of the approximations of each individual term.

To discuss the finite difference approximation of the flexure equation, we define

$$\phi = \frac{D}{\sqrt{1 - w_s^2}} \tag{5.4}$$

$$\psi = \left(\frac{w_s}{\sqrt{1 - w_s^2}} \int_0^s q_v ds + \int_0^s q_h ds \right) \tag{5.5}$$

where ϕ and ψ are the coefficients of the fourth and second order terms of Equation 4.36, respectively. We use the subscript $(i+n)$ to denote a term's value at position $(s+n\cdot ds)$. Thus, the finite difference approximation of the flexure equation has the form

$$(\phi_{i-1})w_{i-2}+(\psi_i-2\phi_{i-1}-2\phi_i)w_{i-1}+(-2\psi_i+\phi_{i-1}+4\phi_i+\phi_{i+1})w_i+(\psi_i-2\phi_i-2\phi_{i+1})w_{i+1}+(\phi_{i+1})w_{i+2}=[q_n] \tag{5.6}$$

Although the flexure equation does not explicitly contain any zeroth order terms, we extract some from q_n, the net normal force defined in Equation 4.34. The force q_n is composed of both normal pressure and viscous forces. Each of these types of forces has an implicit dependence on deflection (w), the un-differentiated or zeroth order term. The pressure force is proportional to the mass of the material situated above the subducting plate, which is determined in part by the depth to which the plate has deflected. As outlined in Chapter 3, the viscous force is proportional to the velocity at which the plate moves relative to the mantle, which is a function of the change in deflection, $(w_{t+\Delta t}-w_t)$, where w_t represents the past, known deflection and $w_{t+\Delta t}$ represents the deflection to be currently calculated by the flexure equation. Thus, we can split the terms comprising q_n into two main groups, one that depends on deflection w and one that does not. We can then write the w-dependent group as a single coefficient, χ, multiplied by w. The other group may be represented by a lone constant, ξ. This slightly changes the appearance of the finite difference approximation of the flexure equation to

$$(\phi_{i-1})w_{i-2}+(\psi_i-2\phi_{i-1}-2\phi_i)w_{i-1}+(\chi_i-2\psi_i+\phi_{i-1}+4\phi_i+\phi_{i+1})w_i+(\psi_i-2\phi_i-2\phi_{i+1})w_{i+1}+(\phi_{i+1})w_{i+2}=\xi \tag{5.7}$$

Collecting the coefficients, we can rewrite Equation 5.7 as

$$Aw_{i-2}+Bw_{i-1}+Cw_i+Dw_{i+1}+Ew_{i+2}=\xi \tag{5.8}$$

The solutions to the above finite difference equation represent the results of our model and are computed by the program described below.

5.3 The Code

At the heart of our model of subduction is a *FORTRAN 90* code designed to solve the flexure equation derived in Chapter 4 under the conditions described in Chapter 3 in order to understand the problems outlined in Chapter 2 [see Appendix B for a copy of the code]. The code receives a set of parameters defining the initial state of the subduction system, uses the parameters to solve the finite difference approximation of the flexure equation, outputs the solution describing the new state (new deflection) of the subduction system, then steps through time, re-solving the flexure equation at each step to show the temporal evolution of subduction. First, the code opens and reads an input file that contains dimensionalized parameters that define the initial configuration of the subducting plate as well as the physical properties of the subducting plate, the overriding plate, and the mantle. These parameters include

- time (Δt) between each computation [Ma]
- total duration (t) of model run [Ma]
- number of nodes (N) along the subducting plate at which the deflection will be computed
- distance (Δs) between each node, where $\Delta s \cdot N =$ total plate length [km]
- initial position (deflection w) of the subducting plate [km]
- flexural rigidity (D) of the subducting plate
- initial depth of water above the subducting oceanic plate (which later translates to density of subducting lithosphere) [km]
- initial elevation/water depth of overriding continental plate (also translates to density) [km]

- viscosity (μ) of mantle [$\mu = 10^{21} Pa \cdot s$]
- length scaling (γ) of viscous forces [km]
- velocity (v_m) of mantle [$\frac{mm}{yr}$, positive toward the right]

While many of these parameters are varied throughout this study, we consistently use $\Delta t = 0.01$ [Ma], $t = 150$ [Ma], $N = 991$, and $\Delta s = 10$ [km], giving a total slab length ($N \cdot \Delta s$) of 9910 kilometers. When non-dimensionalized, the length and time increments satisfy the numerical stability criterion of

$$\frac{\Delta t}{\Delta s^2} \leq \frac{1}{4} \tag{5.9}$$

Next, the code defines a few key physical constants to be used later, such as

- g = 9.8 $\frac{m}{s^2}$
- $\rho_{crust} = 2700 \frac{kg}{m^3}$
- $\rho_{asthenosphere} = 3200 \frac{kg}{m^3}$
- $\rho_{water} = 1000 \frac{kg}{m^3}$
- $\rho_{mantle} = f(\rho_{crust}, \rho_{asthenosphere}, \rho_{water})$

Finally, the code converts all of these constants and input parameters into MKS (Meters/Kilograms/Seconds) units and then non-dimensionalizes them. Parameters like initial deflection, flexural rigidity, and density are assigned to each node along the subducting plate and are stored in arrays of size N. Similar arrays are generated for the $sine(w_s)$ and $cosine\left(\sqrt{1 - w_s^2}\right)$ of the angular deflection, since these factors appear throughout the flexure equation. A forward difference is used to calculate w_s, since it is a differential of an odd order.

Next, the code defines the viscosity structure of the mantle. Here, we may model the mantle with a constant viscosity or a viscosity that increases with depth, either linearly or exponentially. We may also treat the mantle's viscosity as a step-function

that increases sharply at the lower mantle boundary or at any number of specified depths.

Now, the model is completely set up, and we are prepared to begin solving the finite difference equation used to approximate the differential equation of flexure. The finite difference equation derived in the previous section can also be thought of as a matrix equation

$$Mx = y \tag{5.10}$$

where M is a band matrix that holds the known coefficients (A through E) of the finite difference equation along its diagonals, x is a column vector containing the new or unknown deflection at each node ($w_1, w_2, w_3, ..., w_N$), and y is a column vector containing the set of known constant coefficients at each node ($\xi_1, \xi_2, \xi_3, ..., \xi_N$). To solve the finite difference equation and thus find the deflection under a certain set of conditions, we can solve the matrix equation 5.10 for x by inverting the matrix M and taking

$$x = yM^{-1} \tag{5.11}$$

In order to accomplish this, the code must, for each node, first find the coefficients, A through E (comprised by terms ϕ, ψ, and χ), of the band matrix M, as well as the constant term, ξ, of the vector y. The terms ϕ, χ, and ξ are all calculated within one loop, while the integrals of ψ are calculated in a separate loop [see commented code in Appendix B for details]. If we were to treat the velocities that generate the viscous forces found within ψ the same way we did those found in q_n, the finite difference approximation would then have a fourth-order term multiplied by a zeroth-order term, greatly complicating the task of finding even numerical solutions to the flexure equation. To avoid this complication, we designate the velocity of each node at the current timestep, $(t + \Delta t)$, equivalent to the velocity at the last timestep, t, which itself is related to the change in position from time $(t - \Delta t)$ to time t. For the models initial timestep, the velocities are taken to be zero.

After computing terms ϕ, ψ, and χ, the code combines them as shown in the previous section to yield the band matrix coefficients of A, B, C, D, and E. A subroutine uses these coefficients, which define M, along with the constant ξ, which defines y, to solve the matrix equation given in 5.11 for the unknown, x. This yields the current deflection, w, at each node as a function of the nodes position, s. However, this functional relationship only specifies the vertical and along-plate distances between two nodes; it contains no information about the horizontal spacing between nodes. In order to specify a new x-coordinate for each node, we must control the direction of the nodes motion from the past deflection, where the x-coordinate was known, to the new deflection. We do this by assuming that the motion of the lithosphere through the mantle reaches a steady-state rate and direction during the early stages of the model run, perhaps after a certain critical length of lithosphere has been subducted. Each node is thus moved in the steady-state direction from its old position to its new position, thereby providing the node with a specified x-coordinate and the subducting plate with a specified shape.

The deflections and corresponding x-positions calculated by the above procedures may yield configurations in which some nodes are not equally spaced at the initially specified distance (Δs), thus effectively squeezing or stretching the subducting lithosphere. To counteract this effect of the numerical computation, the code contains a short procedure to slide nodes along the length of the subducting plate to positions that ensure equal node spacing and constant plate length. Once all nodes have been assigned their final positions, all velocity vectors and vector components are calculated by comparing the new node positions to the positions from the previous timestep. These velocities are then saved for the next timestep, where they are used to compute the viscous forces in ψ, the second order coefficient in the finite difference approximation of the flexure equation, previously shown as equation 5.7.

At each initially specified time increment, defined as some multiple of Δt, the code prints data related to the deflection results to a set of output files. One of these output files lists the index (an integer), deflection (w), and x-coordinate of each node. By plotting w versus x for every node, we create an image of the subducting plate.

In our model, the end of the slab at $s = 0$ km is free whereas the opposite end, at $s = 9910$ km is fixed. Consequently, as more of the slab subducts into the mantle, the surface expression of the subduction zone, or the subduction boundary, retreats back toward the fixed end of the slab.

Chapter 6

Model Results for Subduction of Oceanic Lithosphere

6.1 Deflection vs. Position Results

Our mission is to develop a better understanding of the causes and evolution of deformation in the upper plate of a subduction system. We focus our study of subduction on the rate at which the subduction boundary retreats and the angle at which the lithospheric slab subducts, since these two factors seem intimately related to back-arc extension and other modes of upper plate deformation. Specifically, we are interested in learning what forces or physical parameters might control retreat rates and subduction angles. The questions we aim to answer include:

1) How do the viscous forces applied to the elastic slab by the viscous mantle affect retreat rates? How do the viscous forces affect subduction angles?

2) Do the normal and shear viscous forces differ in their effects? What are these differences?

3) How do the influences of the viscous forces vary from a situation in which the mantle is stationary to a situation in which the mantle is mobile?

4) How does the density (initial water depth, w_o) of the downgoing lithosphere affect retreat rates and subduction angles? What are the time scales of these effects?

To find answers to these questions, we examine the results of the physical model

constructed in Chapter 3, which is implemented by the *FORTRAN 90* code outlined in Chapter 5. The code uses a set of input parameters and initial conditions to compute a subducting slab's deflection (w) as a function of position along the slab (s) through a succession of time steps. Deflection vs. position results are plotted at specified time increments, utilizing the coordinate system described in Chapter 4. These deflection vs. position plots represent two-dimensional cross-sections through evolving subduction zones. At each time step, we can use the cross-section to measure the angle at which the subducting slab descends into the mantle. We can also measure the distance the subduction boundary travels between each time step in order to calculate the retreat rate. The two-dimensional cross-section images can also tell us something about the general behavior of a subducting slab. For example, we can observe what happens to a subducting slab when it reaches the boundary of the high-viscosity lower mantle, at a depth of about 600 kilometers.

6.2 Results for Stationary Mantle

To begin our investigation of the topics mentioned above, we first apply our subduction model to a simple scenario, in which a dense slab of oceanic lithosphere subducts into a viscous mantle that is stationary relative to the fixed end of the slab. In terms of the numerical computation outlined in the previous chapter, the dense oceanic lithosphere has an initial water depth (w_o) of 6.0 kilometers, and the mantle is given a velocity (v_m) of zero mm/yr. Every model run lasts exactly 150 million years.

The oceanic slab is fixed at the extreme right of the two-dimensional cross-section, where $s = 9910$ kilometers. The opposite end of the slab ($s = 0$ km) is free and is given an initial deflection of 600 kilometers. The initial deflection decreases linearly from 600 km at the free end to zero km at $s = 1000$ kilometers, resulting in an initial angle of subduction of about 37 degrees. Everywhere between that "hinge" point ($s = 1000$ km) and the fixed end of the slab, the deflection is zero and the value of the x-coordinate is equivalent to the value of the s-coordinate.

As the numerical model built into the *FORTRAN 90* code starts to run, the

very dense, negatively buoyant oceanic lithosphere begins to descend into the stationary mantle. Pressure and gravitational forces tend to push the lithosphere down into the mantle. As detailed in Chapter 3, the mantle responds by exerting viscous forces opposite the direction of relative motion between it and the subducting lithosphere. Although these forces are manifest as both shear and normal viscous forces, we first examine the effects of the normal viscous forces because intuitively, it seems as though the normal component of a subducting slab's motion through the mantle would outweigh the parallel (shear) component.

6.2.1 Effects of Normal Viscous Force

To use our numerical model to examine the normal viscous forces only, we simply set the effective shear viscosity to zero. This is actually accomplished by giving the effective shear viscosity an infinite length scaling factor, γ_S (the " γ " scaling factors are described in Chapter 5). The length scaling factor for the normal viscous force is made finite.

Figure A-6 presents a two-dimensional cross-sectional view of the the evolution of the of a dense oceanic slab subducting into an mantle with a viscous length scale $\gamma_N = 20$ km. The horizontal line at $y = 0$ km represents the undeflected portion of the oceanic lithosphere. The initial position of the pre-deflected slab is plotted to the extreme left. Each oblique line to the right of the initial slab position represents the new position of the slab, plotted at 10 million year increments through a total of 150 million years (or until the entire lithosphere has been consumed). The horizontal line at $y = 600$ km represents lithosphere that has been deeply subducted and has come to rest along the upper boundary of the highly viscous lower mantle. This occurs for all model runs in which the mantle is stationary; without additional motion of the mantle relative to the fixed end of the lithosphere, the subducting slabs in our model are unable to penetrate the upper boundary of the lower mantle.

We can glean a great deal of information from the two-dimensional cross-sectional view. Some immediate observations include:

1) The subducting slab eventually assumes an overall angle much shallower than

its initial angle (37°).

2) Once it is attained, the shallow angle of subduction is approximately constant throughout the duration of the model run (at least until the model "runs out" of lithosphere to subduct.)

3) The distance covered by the subducting slab between each time step is also approximately constant.

We investigate these observations in greater detail by using the *FORTRAN 90* code to compute and plot the actual angle of subduction and the rate of retreat of the subduction boundary. We measure the angle of subduction at a depth of 300 km since, around that depth, the subducting slab is relatively straight and gives a good indication of the average angle between itself and the horizontal. We define the rate of retreat as the horizontal velocity of the point farthest from the free slab end where the upper surface of the slab is in contact with the mantle. The horizontal velocity is simply the distance traveled by that point along the x-axis from one time step to the next, divided by the amount of time passed between the two time steps.

The curves in Figure A-7 represent the rate of subduction boundary retreat plotted against time for an infinite γ_S (no shear forces) and a variety of γ_N values. From top to bottom, the retreat rate curves result from γ_N = 45, 40, 35, 30, 25, and 20 km, respectively. Each curve follows a common pattern in which the retreat rate starts at zero mm/yr at $t = 0$ Ma, increases sharply over a span of about 5 Ma, then increases slowly for another 5 to 10 Ma until it plateaus at a "steady-state" retreat rate. Once the steady-state retreat rate is achieved, after a total of about 10 to 20 Ma have passed, it remains constant for the remainder of the model run. This constant retreat rate explains the equal spacing between successive slab positions shown in Figure A-6. Other effects of this "steady-state" will be discussed later.

The steady-state retreat rates displayed in Figure A-7 vary almost linearly with γ_N from a minimum (at γ_N = 20 km) of $\sim$ 100 mm/yr to a maximum (at γ_N = 45 km) of $\sim$ 230 mm/yr. This maximum retreat rate approaches the fastest plate motion ever measured, which is $\sim$ 240 mm/yr, at the Tonga Trench subduction zone [1]. The faster a subduction boundary retreats, the more quickly it reaches its steady-state

rate; for a slab retreating at $\sim$ 100 mm/yr (γ_N = 20 km), the steady-state retreat rate is reached after $\sim$ 20 Ma, whereas for a slab retreating at $\sim$ 230 mm/yr (γ_N = 45 km), the steady-state retreat rate is reached after $\sim$ 12 Ma.

Figure A-8 illustrates the linear relationship between γ_N and retreat rate, which roughly follows the equation $5 \cdot 10^{-6}(yr^{-1}) \cdot \gamma_N(m)$ = rate of retreat (m). As expected, decreasing γ_N heightens the mantle's viscous resistance to the subducting slab's motion, thus directly decreasing the steady-state retreat rate.

While it is relatively clear that the normal viscous force applied to the lithosphere by the mantle should affect the rate at which a subduction boundary retreats, the influence of this force on the angle of subduction is less straightforward. Would the normal viscous force add support to a subducting slab, causing it to descend into the mantle at a shallow angle? Also, since the normal viscous force has such a great influence on the steady-state rate of retreat, will it have an equally large influence on the steady-state angle as well?

The curves in Figure A-9 represent the angle of subduction plotted against time for an infinite γ_S (no shear forces) and a variety of γ_N values. From left to right, the subduction angle curves result from γ_N = 45, 40, 35, 30, 25, and 20 km, respectively. As observed with the retreat rate curves, each subduction angle curve begins with a steep gradient that quickly shallows to a steady-state subduction angle that persists for the remainder of the model run. Unlike the rate of retreat however, for $\gamma_S = \infty$, the steady-state angle of subduction does not vary significantly with γ_N. As shown in Figure A-9, the angle of subduction remains constant at $\sim$ 24 degrees regardless of the value of γ_N. Thus, for a stationary mantle, it appears as though changes in the normal viscous force alone do not alter the angle at which a slab of oceanic lithosphere subducts. Geophysical studies of real subduction zones have found that lithospheric slabs may descend at angles as shallow as 10 degrees or as steep as 70 degrees [2]. Therefore, we expect to find some means by which the angle of a subducting slab's descent may be affected, either positively or negatively.

6.2.2 Implications of "Steady-State" Subduction

Before proceeding further into our examination of the results of our subduction model, we would like to briefly discuss the importance of the observation that our modeled subduction zones attain a "steady-state" only a few million years into each run. The steady-state at which both retreat rate and subduction angle remain constant does not merely act as a convenient measuring point; the presence of a steady-state provides us with some very useful information about the process of subduction. Because the slabs reach steady-state such a short time after being released from their initially imbalanced condition, we can justifiably use the uniform motion implied by steady-state subduction to "fine tune" the numerical computation of the lithosphere's deflection. (To avoid any circularity in this argument, we have found that steady-state is reached whether we initially assume steady-state motion or not).

Figure A-10 demonstrates that for a slab in steady-state subducting at an angle α, a point along that slab moves in a direction directly related to α. Specifically, each point on a subducting slab in steady-state will move down and toward the right along a vector that makes an angle of $\theta = \frac{\alpha}{2}$ with the vertical (or an angle of $\phi = 90 - \frac{\alpha}{2}$ relative to the portion of the slab that extends below the node). As a point on the slab moves through the mantle in this manner, it experiences viscous forces that are proportional in size to the magnitude of the its velocity.

The total velocity of a point on a slab can be decomposed into two components, one perpendicular to the subducting slab and one parallel to the slab. These two velocity components, and thus the normal and shear viscous forces for which they are responsible, are related through Vn_{tot} to the subduction angle (α). For shallow α, the angle between a node's total velocity vector and the slab ($90 - \frac{\alpha}{2}$) will be high. As a result, the perpendicular component of the node's velocity will be significantly larger than the parallel velocity component. Therefore, unless γ_S is significantly smaller than γ_N, the magnitude of the normal viscous force should exceed that of the shear viscous force. Of course, for very steep subduction angles (α approaching 90° , $\frac{\alpha}{2}$ approaching 45°), the shear and normal viscous forces will be nearly equivalent if γ_S

and γ_N are approximately equal.

6.2.3 Effects of Shear Viscous Force

Up to now, we have not yet experimented with the shear viscous force. Now we will begin to test its effects on retreat rate and subduction angle by adding it to the normal viscous force. For the normal viscous force, we use $\gamma_N = 20$ km, since that value produced both a reasonable retreat rate (~ 100 mm/yr) and stable numerical solutions to the finite difference approximation of the flexure equation. To add the shear viscous force into our numerical model of subduction, we must assign it a non-zero effective shear viscosity. We accomplish this by using a variety of finite values, ranging from 200 to 50 kilometers, for the length-scaling factor (γ_S). At $\gamma_S = 200$ km, the effects of the shear viscous force begin to reveal themselves. As the length of γ_S shrinks beneath 50 km, the numerical solutions produced by the *FORTRAN 90* code begin to experience instabilities that could not be eliminated within the time constraints of this thesis.

The curves in Figure A-11 represent the rate of subduction boundary retreat plotted against time for $\gamma_N = 20$ km and various γ_S values. From top to bottom, the retreat rate curves result from $\gamma_S = \infty$, 200, 100, and 50 km, respectively. Similar to the previous case, when only the normal viscous force was involved, retreat rates reach a steady-state after approximately 20 Ma. Also, just as an increased normal viscous force (reduced γ_N) slows steady-state retreat rates, we find that for a constant γ_N, the progressive addition of the shear viscous force (performed by decreasing γ_S) leads to a further reduction of the steady-state retreat rate. With γ_N constant at 20 km and an infinite γ_S, the steady-state retreat rate is $\sim$ 101 mm/yr. When γ_S is reduced to 200 km, the steady-state retreat rate drops to 99 mm/yr, and when γ_S is reduced to 50 km, the steady-state retreat rate drops to $\sim$ 94 mm/yr.

However, unlike the relationship between γ_N and steady-state retreat rate, the curves shown in Figure A-11 seem to indicate that for constant γ_N, the relationship between γ_S and steady-state retreat rate is not linear. Figure A-12 illustrates this non-linear relationship. Probable causes for the difference in the relationships between

γ_S and steady-state retreat rate and γ_N and steady-state retreat rate are discussed below.

As we have seen in the previous section, when the mantle is stationary, the normal viscous force seems to have no effect on the angle of subduction. Now we look at what happens to the angle of subduction when the shear viscous force is applied to a slab of lithosphere subducting through a stationary mantle. The curves in Figure A-13, from top to bottom, represent the angle of subduction plotted against time for γ_S values of 50 km, 100 km, 200 km, and infinity, respectively. Again, we hold γ_N constant at 20 km. As before, the curve representing the subduction angle when $\gamma_S = \infty$ and $\gamma_N = 20$ km reaches a steady-state value of $\sim$ 24 degrees. However, as γ_S is decreased to 200 km and less, the angle of subduction begins to steepen, reaching a value $\sim$ 26 degrees when $\gamma_S = 50$ km. Figure A-14 shows the steady-state subduction angle plotted as a function of γ_S. Like the steady-state rate of retreat, the steady-state subduction angle is not linearly proportional to γ_S. Changes in γ_S will be most important when γ_S is small because the steeper the angle of subduction the greater the effect of the shear viscous stress on that angle will be on the slab.

6.3 Results for Moving Mantle

In the first half of this chapter, we explore the effects of the viscous forces on a slab of oceanic lithosphere subducting into an mantle that is stationary relative to the fixed end of the oceanic lithosphere. In general, the normal viscous force applied by the mantle to the bottom of a sinking slab exerted a large influence on the steady-state retreat rate while having no detectable effect on the steady-state subduction angle. The shear viscous force, generated by a slab-parallel velocity component that is smaller than the slab-perpendicular component (due to steady-state motion at a shallow α), had a moderate effect on the steady-state retreat rate and a small but perceptible effect on the steady-state subduction angle.

The relative importance of the normal and shear viscous forces may change when the mantle is set into motion. Though the slab-parallel component of a slab's velocity

relative to a stationary mantle is small for shallowly subducting slabs, the slab-parallel velocity of the horizontally moving mantle relative to a shallowly subducting slab might be greater than its slab-perpendicular velocity component. In this case, the shear viscous force could be larger than the normal viscous force, thus enhancing the aforementioned effects of the shear viscous force.

6.3.1 Effects of Normal Viscous Force

As in our examination of the subduction of oceanic lithosphere into a stationary mantle, we will begin our investigation of subduction into a mobile mantle by initially considering only the normal viscous forces. Therefore, for now, we set $\gamma_S = \infty$. For all model runs with a mobile mantle, we will continue to use $\gamma_N = 20$ km.

We give the now-mobile mantle a positive velocity (v_m) toward the right, in the direction of increasing x-coordinate. Asthenospheric velocities between 0 and 50 mm/yr are sufficient to produce interesting, feasible, and numerically stable results. This is true for situations involving only the normal viscous force as well as situations involving both the normal and shear viscous forces.

Figure A-15 illustrates a two-dimensional cross-sectional view of the evolution of a slab subducting through an mantle moving toward the right at a velocity $v_m = 10$ mm/yr, with $\gamma_N = 20$ km and $\gamma_S = \infty$. Compare this cross-section to that displayed in Figure A-6. Both cross-sections show slabs dipping into the mantle at angles of ~ 24 degrees. However, the subduction boundary in Figure A-15 retreats slightly faster toward the right than the boundary shown in Figure A-6. Most striking though, is that the subducting slab in Figure A-15 penetrates the boundary at 600 km depth and begins to descend into the lower mantle. Penetration of the lower mantle occurs in our model for v_m as low as 1 or 2 mm/yr (toward the right). This observation seems to indicate that even though the lower mantle's viscosity might be significantly higher than the upper mantle's viscosity, the viscous forces generated by motion (convection) within the mantle may help a slab of lithosphere subduct through the upper-lower mantle boundary. According to recent tomographic imagery produced by Van der Hilst, et al, subducting slabs do appear to descend to depths much greater than 600

kilometers [8].

The uppermost line in Figure A-16 represents a subducting slab's steady-state retreat rate plotted against mantle velocities from 0 mm/yr to 50 mm/yr, when $\gamma_N = 20$ km and $\gamma_S = \infty$. As we have seen before, the steady-state retreat rate for $Va = 0$ mm/yr (stationary mantle) is $\sim$ 101 mm/yr. When the velocity of the mantle increases, so does the normal viscous force applied to the slab's surface. The normal viscous force has a significant downward component, especially for shallowly subducting slabs, so a strengthened normal viscous force should cause the slab to descend more quickly. Since the lithosphere is fixed at its opposite end, the steady-state retreat rate should increase in response to faster subduction. This response is shown by the uppermost line in Figure A-16, which shows the steady-state retreat rate increasing linearly with increasing v_m. In fact, the amount of increase in the steady-state retreat rate from a stationary mantle (retreat rate = $\sim$ 101 mm/yr) to any non-zero mantle velocity is approximately equal to the size of the non-zero velocity. For example, the retreat rate at $Va = 30$ mm/yr is nearly 130 mm/yr, and the retreat rate at $Va = 50$ mm/yr is almost 150 mm/yr.

The steady-state angle of subduction is plotted against mantle velocities from 0 mm/yr to 50 mm/yr, for $\gamma_N = 20$ km and $\gamma_S = \infty$, in the lowest line of Figure A-17. When the mantle was stationary, we found that increasing the normal viscous force had no noticeable effect on the steady-state angle of subduction. According to the lowest line of Figure A-17 however, a moving mantle can force our modeled slab to subduct at a slightly shallower angle. Although the effect of the normal viscous force on the angle of subduction is now measurable, it is nevertheless very small; an mantle moving at a moderate rate of 50 mm/yr reduces the angle of subduction by about one tenth of one degree. Though in the opposite direction, this effect is much less than that which the shear viscous force has on the steady-state angle of subduction for a stationary mantle. Earlier, we showed that when $\gamma_S = 50$ km, the shear viscous force increases the steady-state subduction from $\sim$ 24 degrees to $\sim$ 26 degrees.

6.3.2 Effects of Shear Viscous Force

Since the shear viscous force has a notable effect on steady-state subduction angle when the mantle is stationary, we suspect that a moving mantle, which would generate additional shear viscous forces, might induce an even greater effect on the angle. We illustrate the effect of the shear viscous force on the steady-state angle of subduction and compare it to the effect of the normal viscous force in Figure A-17. As mentioned previously, the lowest line represents the steady-state angle plotted against v_m for $\gamma_N = 20$ km and $\gamma_S = \infty$. Moving upward through Figure A-17, the lines represent steady-state angle vs. v_m for γ_S values of 200, 100, 75, 62.5, 55, and 50 km, respectively. We hold γ_N constant at 20 km.

Two trends can be observed in this particular figure. One trend is that for a given value of v_m, the steady-state angle of subduction increases when γ_S decreases. This correlation between γ_S and the steady-state angle of subduction was apparent even for a stationary mantle, but now it is even more pronounced. The second, more dramatic trend is that when the shear viscous force is present (when γ_S is finite), the steady-state angle of subduction also increases with increasing mantle velocity. The upper line of Figure A-17 illustrates this trend for $\gamma_S = 50$ km; an mantle velocity of 10 mm/yr increases the steady-state angle of subduction from $\sim$ 26 degrees to nearly 28.5 degrees, while an mantle velocity of 50 mm/yr increases the steady-state subduction angle to nearly 41 degrees.

To understand the effect of the shear viscous force on the steady-state retreat rate, we return to Figure A-16. While the top line is plotted for an infinite γ_S (no shear viscous force), the lines below represent the steady state retreat rate as a function of mantle velocity for γ_S values of 200, 100, 75, 62.5, 55, and 50 km, respectively. Earlier we saw that in the absence of the shear viscous force, a moving mantle adds almost its entire velocity (v_m) to the steady-state retreat rate exhibited by a slab subducting into a stationary mantle. However, as γ_S is decreased and the shear viscous force is added to our model, the amount added to the steady-state retreat rate by a moving mantle is significantly diminished.

For example, when $\gamma_S = 62.5$ km, the steady-state retreat rate increases from $\sim$ 95 mm/yr for a stationary mantle to only $\sim$ 100 mm/yr for an mantle moving at a rate of 50 mm/yr. If we increase the shear viscous force slightly more, using $\gamma_S = 55$ km, the steady state retreat rate remains almost constant at a level just below 95 mm/yr, regardless the velocity of the mantle. Thus, our model shows that for a moving mantle, the shear viscous force might counteract effect of the normal viscous force on the rate of retreat. Shear along the surfaces of a narrow subducting slab could slow the rate at which the slab descends into the mantle, causing a decrease in the overall rate of retreat. Most interestingly, and almost counterintuitively, for $\gamma_S = 50$ km, a moving mantle slows the steady-state retreat rate to a level *below* that of the retreat rate for a stationary mantle. As v_m increases, the steady-state retreat rate slows even more. This shows that where the shear viscous force is very strong ($\gamma_S < 55$ km), an mantle moving in the direction of subduction boundary retreat (in our model, toward the right) might actually *slow* the retreat.

As mentioned earlier, within the amount of time provided for this thesis work, we could not achieve numerically stable results for $\gamma_S <\sim 50$ km. Stability issues also limited the range of testable v_m. For instance, with $\gamma_S = 50$ km, the maximum stable v_m was $\sim$ 50 mm/yr. Were we able to succeed at creating a perfectly stable *FORTRAN* code, we would have liked to set $\gamma_S = \gamma_N$ to see what would happen if the shear and normal viscous forces operated at the same level. Based on the results we did achieve, we expect that when the effective shear and normal viscosities are equivalent, a mobile mantle might lead to very steep angles of subduction, such as those observed naturally.

6.4 Discussion

The model presented in this thesis provides some clues about the forces that affect the process of subduction, which may in turn influence surface tectonics. We concentrated our study on learning which forces affect the rate at which a subduction boundary retreats toward the foreland and the angle at which a slab descends into

the mantle, since these two general characteristics play a large role in determining the style of tectonics exhibited near one of these convergent regimes. By using a finite-difference approximation to numerically solve the flexure equation for a slab of oceanic lithosphere descending into a viscous mantle, we are able to measure these characteristics as we "watch" the evolution of a subduction zone through time and space. What do we see?

A slab of oceanic lithosphere subducting into a stationary mantle makes its descent at an angle ($\sim 24 - 26°$) that is relatively shallow when compared to many of the earth's subduction zones. Changes in the effective viscosity of the normal viscous force applied by the mantle to the slab do not significantly affect this angle when the mantle is stationary. Likewise, a high effective viscosity of the shear viscous force ($\gamma_N = 50$ km) steepens the angle by only one or two degrees. Therefore, it appears as though shallow subduction might be indicative of a lack of significant motions in the mantle, or at least motions in the directed from the back-arc toward the trench. When the mantle is set into motion against the subducting lithospheric slab, changes in the effective normal viscosity still have little effect on the subduction angle, which remains shallow. A large effective shear viscosity ($\gamma_N = 50$ km), however, causes the angle to steepen to ~ 41 degrees when the mantle is moving at 50 mm/yr. How steep an angle might be induced by even higher effective shear viscosities? Could an angle of 90 degrees be reached? Might an angle *greater* than 90 degrees be reached, so that the subducting lithosphere "folds" back on itself? Had we been able to input even greater shear viscous forces (smaller γ_S or higher mantle velocities, v_m) into our numerical computation, we may have been able to examine more closely the range of angles the shear viscous force is capable of producing.

Nevertheless, we have learned that the shear viscous force has a significant impact on the angle of subduction, especially when the mantle is in motion. In the near future, we can adjust our model to explore the results of a situation in which the mantle moves from the trench toward the back-arc (in our model, toward the left). Perhaps a high effective shear viscosity of an mantle moving in this direction would cause subduction to occur at an angle even shallower than the 24° angle found for a

stationary mantle.

Both of the characteristics on which we focused, the angle of subduction and the rate of retreat, reach steady-state quickly. After only $\sim 10 - 20$ million years of subduction, the angle and rate arrive at values that remain stable for as long as subduction continues to take place, uninterrupted. This suggests that subduction zones may respond rapidly to change, such as spatial variations in the strength or density of the subducting slab, or spatial and temporal fluctuations in the patterns of mantle motion. The quickness with which the maximum, steady-state retreat rate takes effect also suggests that slab-rollback and related back-arc extension might begin only a short time after the initiation of subduction or the introduction of variations in the slab's physical properties into the subduction zone.

Although variations in the effective normal viscosity have no apparent effect on the steady-state subduction angle where the mantle is stationary, they impose a significant influence on the steady-state retreat rate. Where the mantle moves relative to the fixed portion of the lithosphere at a rate v_m, the effective normal viscosity is high ($\gamma_N = 20$ km) and the effective shear viscosity is set to zero ($\gamma_S = \infty$), the steady-state retreat rate exceeds the retreat rate for a stationary mantle by a quantity almost equal to v_m. Thus, a rapidly moving mantle might produce high retreat rates. However, this effect is greatly reduced (and possibly even reversed) when the shear viscous force is taken into account (finite γ_S), since it impedes the slab's descent into the mantle and reduces the overall rate of retreat of the subduction boundary.

The behavior of a slab as it reaches the 600 km deep boundary between the upper and lower mantle is also a function of the rate of mantle motion. When the mantle was held motionless, a slab did not penetrate the high-viscosity lower mantle. Instead, once the slab reached a depth of 600 km, it would level out and rest along the surface of the lower mantle. When the mantle was allowed to move at a rate of v_m, the slab penetrated into the lower mantle, even for small v_m. A slab would not dive straight into the lower mantle along the same path as it had traveled through the upper mantle, however; part of the slab would lie horizontally at 600 km while another part of the slab, near the free end, made its descent into the lower mantle.

This change in the slab's behavior suggests that although the negative buoyancy of a dense oceanic slab might not be enough to drag it down into the high-viscosity lower mantle, viscous forces generated by motion in the mantle may help a subducting slab to penetrate the 600 km discontinuity.

Overall, the relatively simple model outlined in this paper yields some interesting insight regarding the differences between the effects of the normal and shear viscous forces. The results of our model reveal the sensitivity to the ratio of the effective shear and normal viscosities in determining the angle at which a slab of oceanic lithosphere subducts. The results also indicate that for a relatively high normal to shear viscosity ratio ($\frac{\gamma_N=20km}{\gamma_S=50km} \longrightarrow$ effective shear viscosity nearly as large as effective normal viscosity), a quickly moving mantle might actually *slow* the rate of subduction boundary retreat rather than increase it.

Our assumption that the viscous forces are directly proportional to the relative velocities between the subducting slab and the surrounding, viscous mantle might not be the most appropriate means of approximating these forces, especially for a subduction zone in which small-scale mantle convection is present. Even if this assumption is not entirely correct, our model does demonstrate the significant effect of the shear viscous force on the steady-state subduction angle and retreat rate, especially under the conditions of a mobile mantle. There are, of course, many aspects of the model that could certainly be performed in a different manner. For instance, we could model the mantle in a number of ways. One of these ways might be to give it a non-uniform viscosity structure, such as one that increases either linearly or exponentially with depth. We might also eliminate the sudden step in viscosity that we have currently placed at the boundary between the upper and lower mantle. Non-Newtonian rheologies might be experimented with as well. Perhaps even more useful would be to model the motion of the mantle in a more complicated fashion, to mimic small-scale convection, rather than having it move only horizontally.

In addition to testing for changes introduced by different types of mantle rheologies, we might also consider other rheologies for the subducting lithosphere. Instead of using a strictly elastic rheology, we might try to model the lithosphere with either

a viscous or visco-elastic rheology.

Another goal is to eliminate the numerical instabilities suffered by our solutions to the finite difference approximation of the flexure equation. Once this problem is removed, we can then see what happens when the effective shear and normal viscosities are truly equal, or perhaps when the effective shear viscosity is greater than the effective normal viscosity. At that point we will finally be able to test the full range of possible subduction angles and retreat rates.

The most interesting way in which we intend to extend this model is by using it to investigate the relationship between the density of the subducting slab and the retreat rate and subduction angle. Preliminary results indicate that the rate of subduction zone retreat is directly proportional slab density; very dense slabs yield high retreat rates. On the other hand, the results show that the angle of subduction is inversely proportional to slab density; very dense slabs subduct at shallower angles than slabs of less density. What we aim to learn with more modeling is how these density related effects combine with the effects due to the viscous forces outlined in this thesis.

Appendix A

Figures

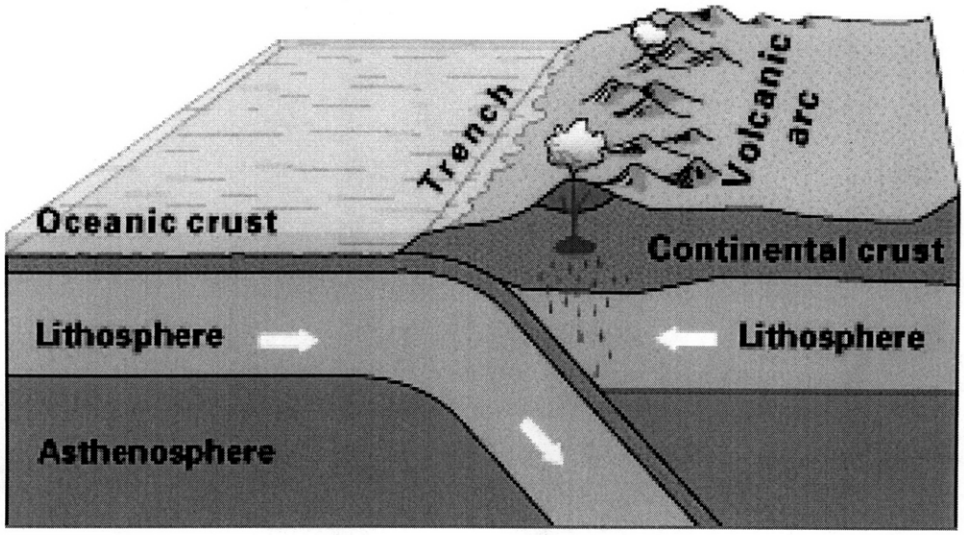

Figure A-1: Cartoon to show the components and structure of a "typical" subduction zone.

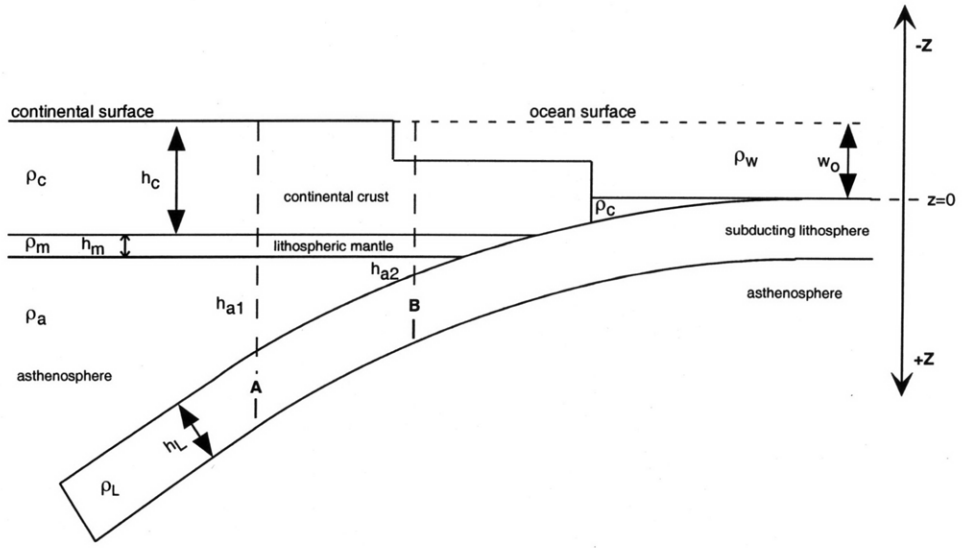

Figure A-2: Illustration of the structure of the overriding continental lithosphere, and the pressure forces applied to the subducting slab.

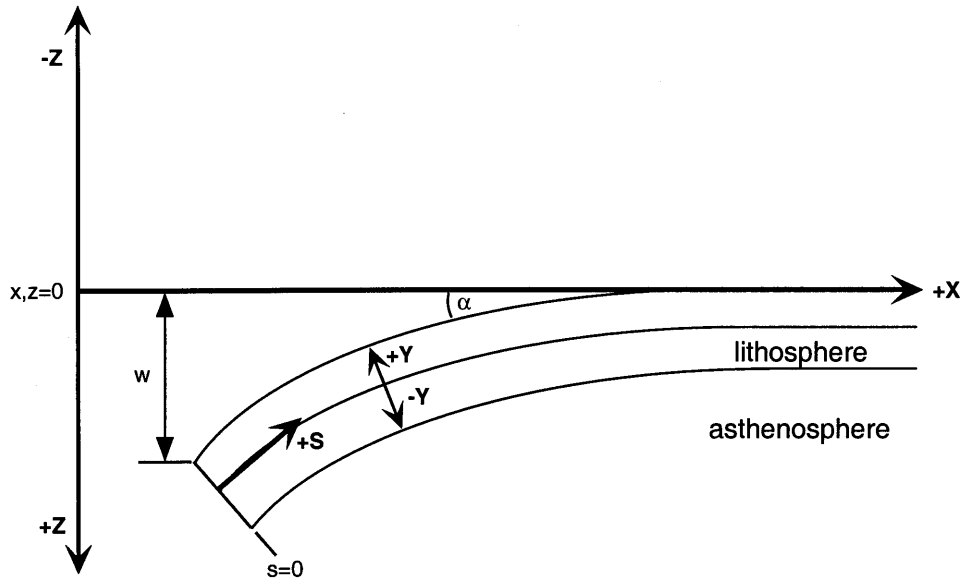

Figure A-3: The coordinate system used in the derivation of the flexure equation.

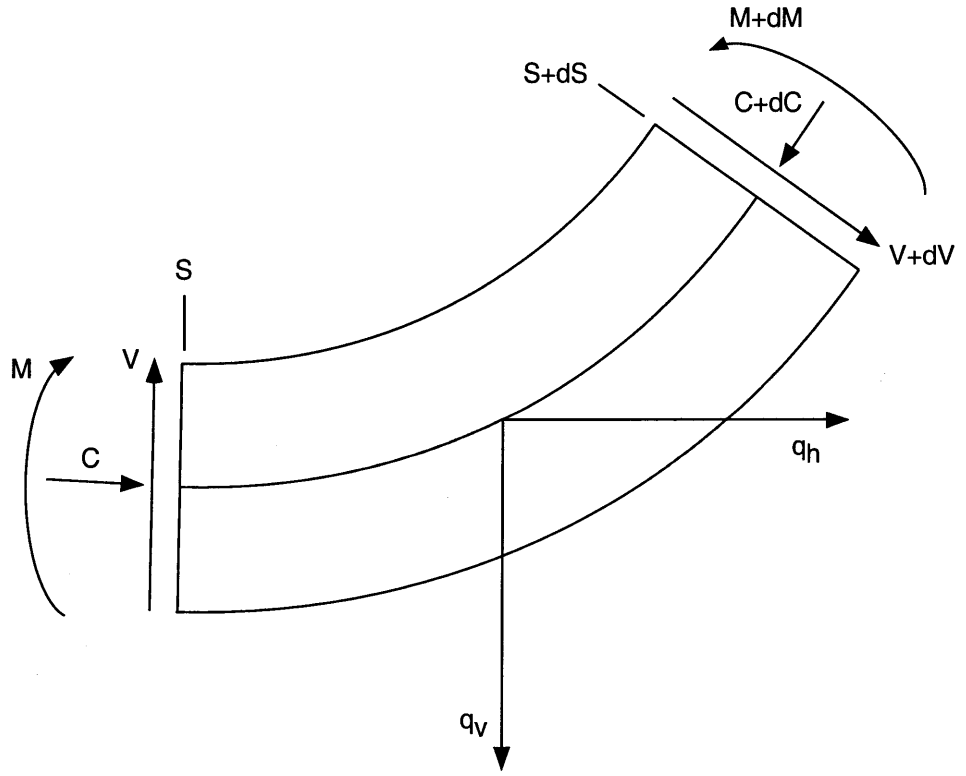

Figure A-4: The forces and torques exerted upon a small segment of deflecting lithosphere.

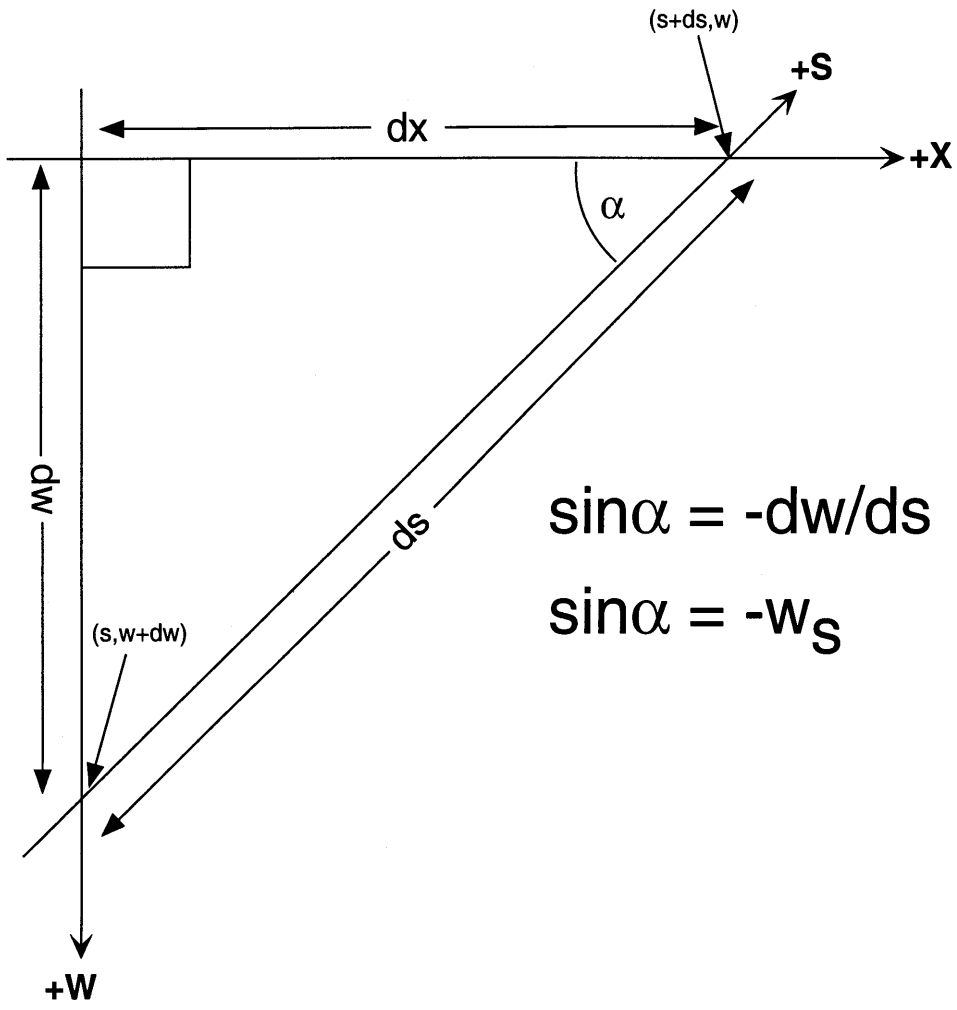

Figure A-5: The geometrical relationship between deflection (w) and subduction angle (α).

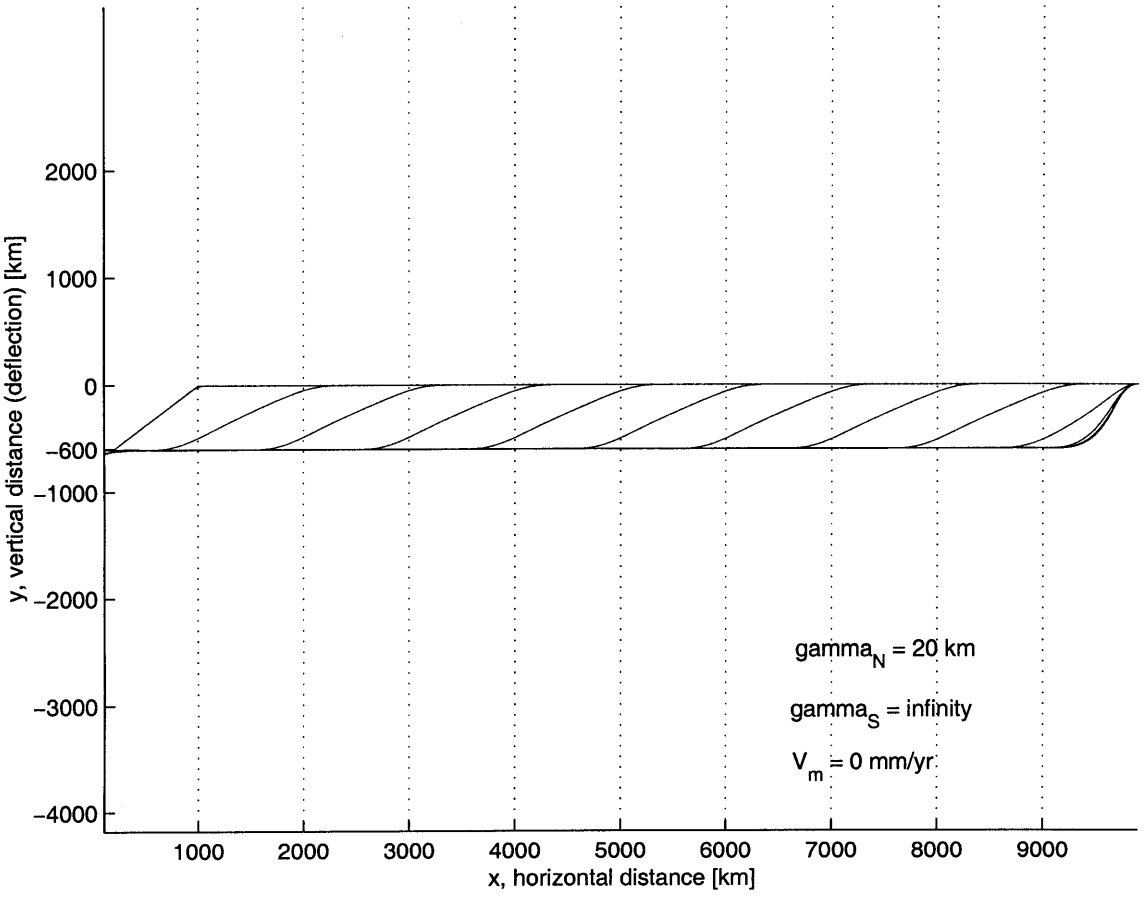

Figure A-6: Two-dimensional cross-sectional view of subduction (Stationary mantle and no shear viscous force). The slab does not subduct deeper than 600 km.

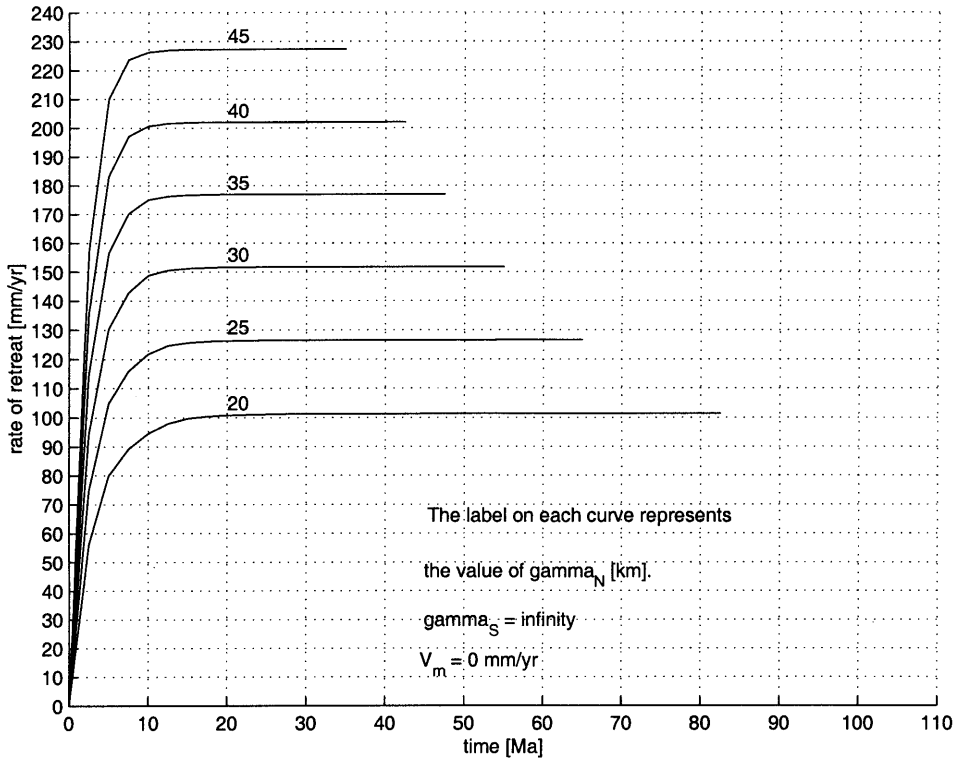

Figure A-7: Rate of retreat of subducting slab plotted against time (Stationary mantle and no shear viscous force).

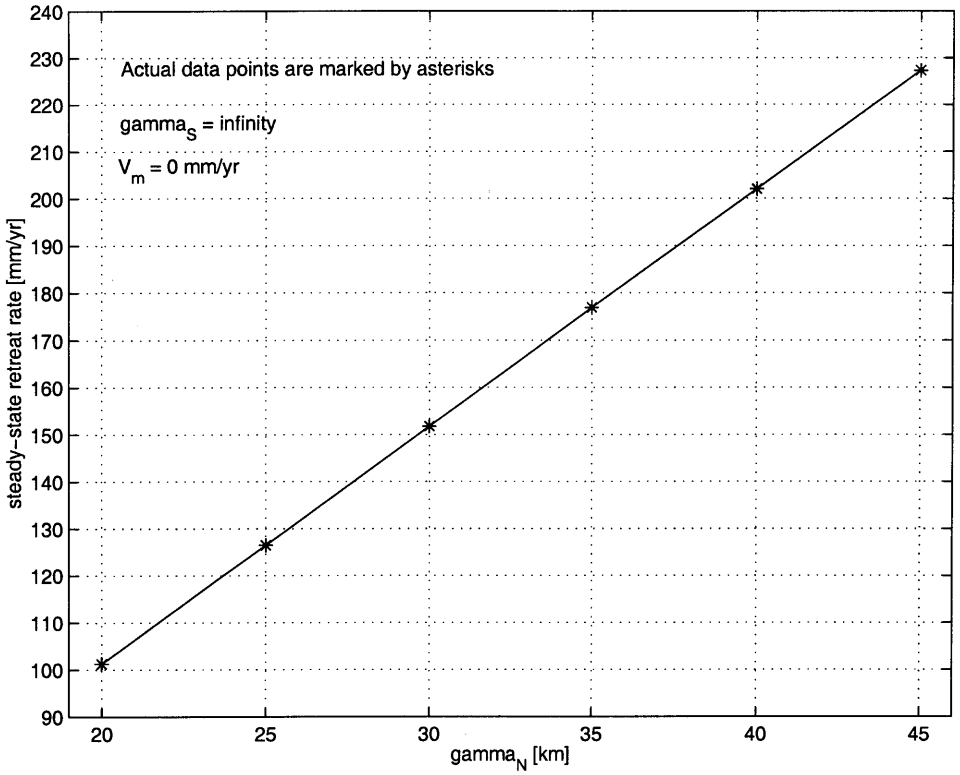

Figure A-8: Steady-state retreat rate plotted against γ_N (Stationary mantle and no shear viscous force).

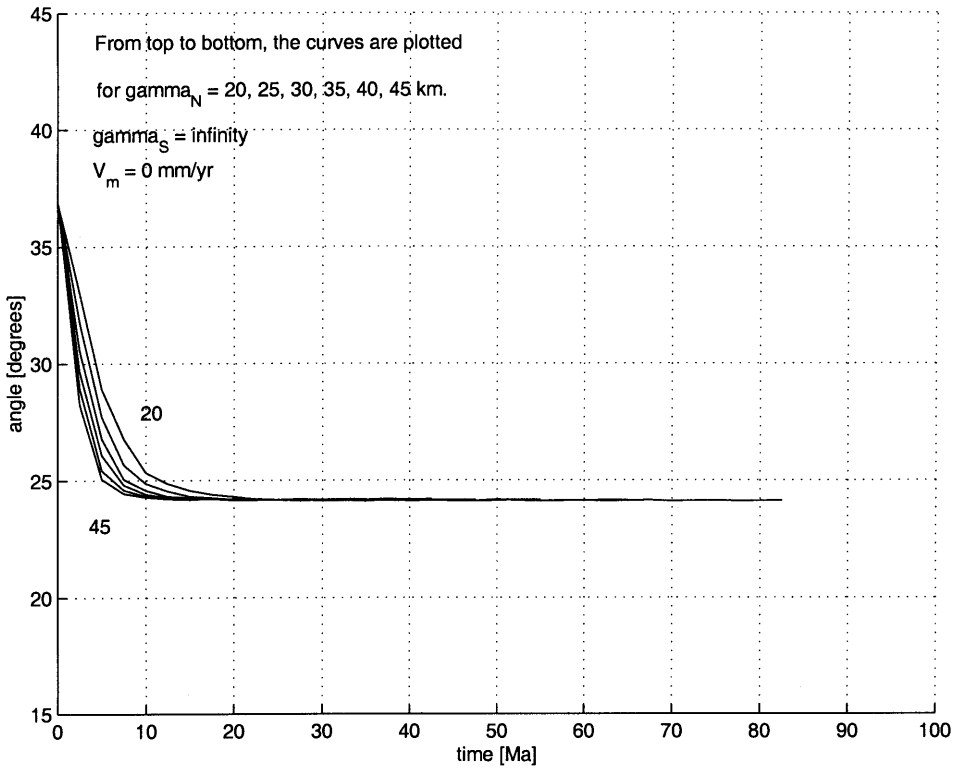

Figure A-9: Angle of subduction plotted against time (Stationary mantle and no shear viscous force).

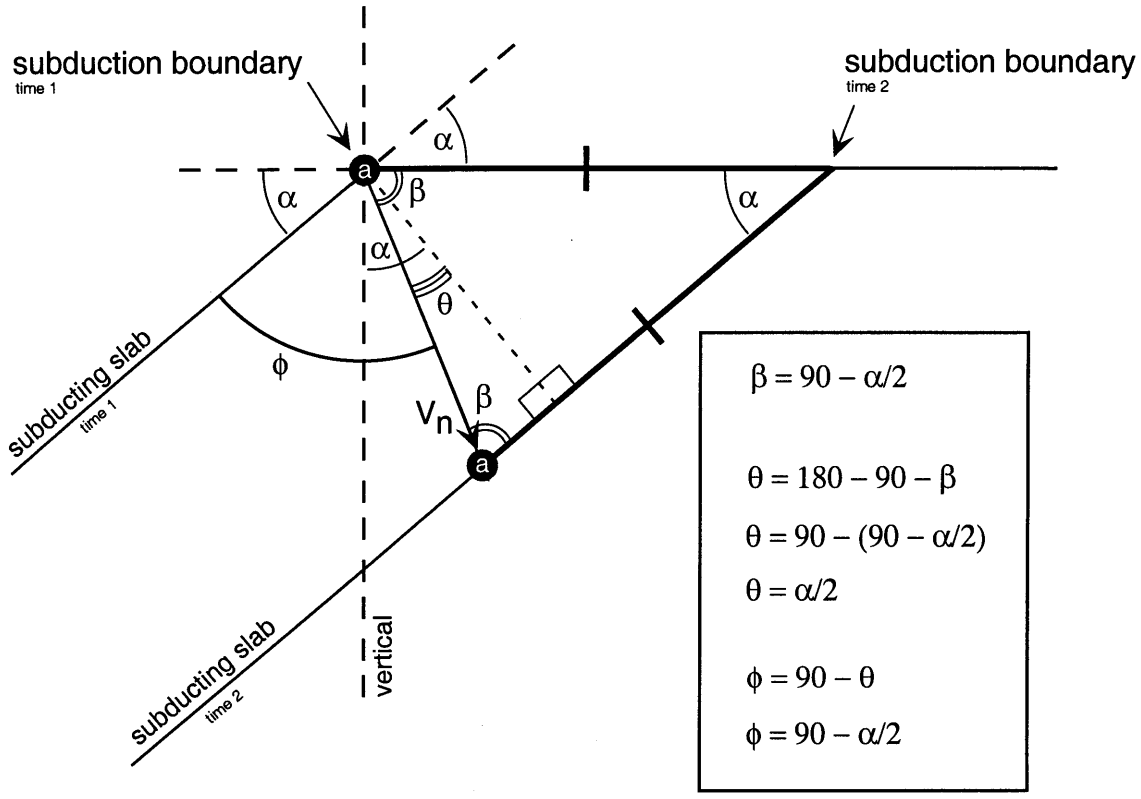

Figure A-10: Diagram to show the direction of motion of a point, (a), on a slab subducting at steady-state (constant rate and angle) through the mantle.

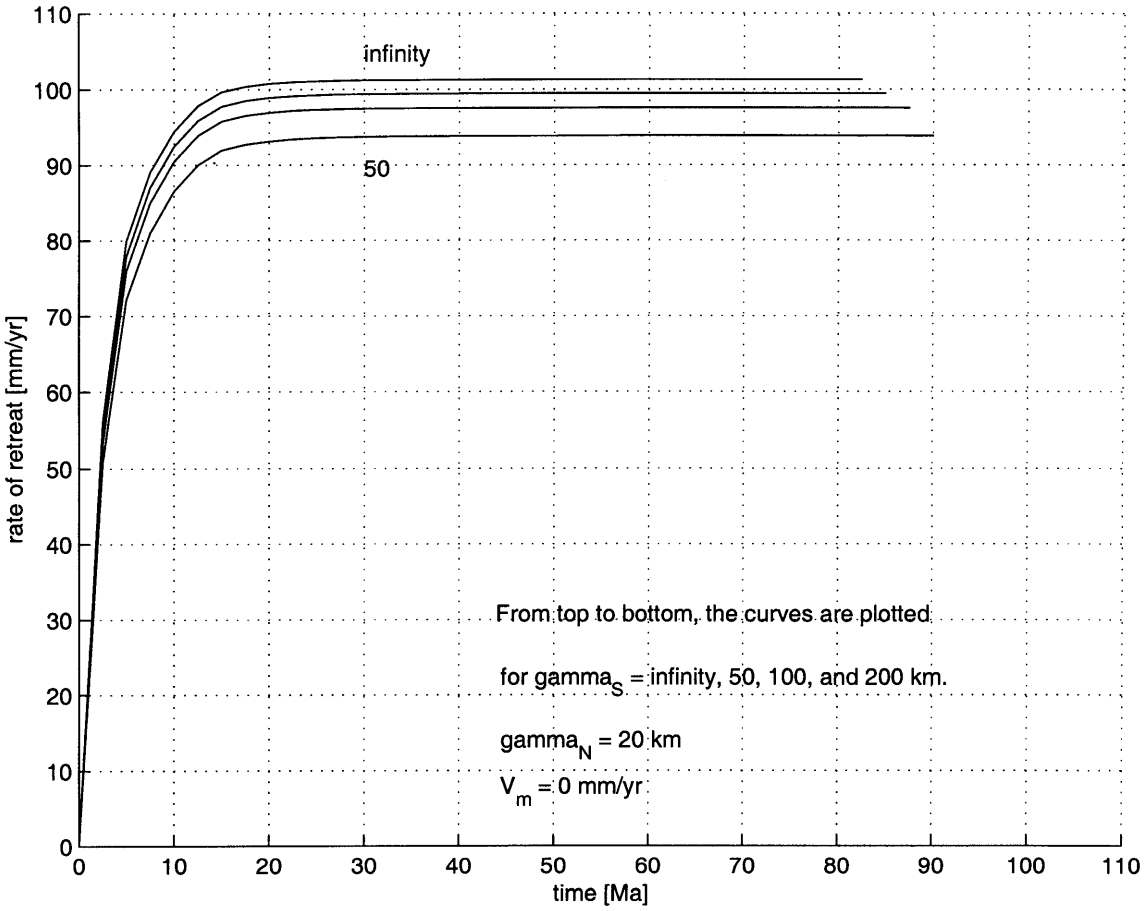

Figure A-11: Rate of retreat of a subducting slab plotted against time (Stationary mantle)

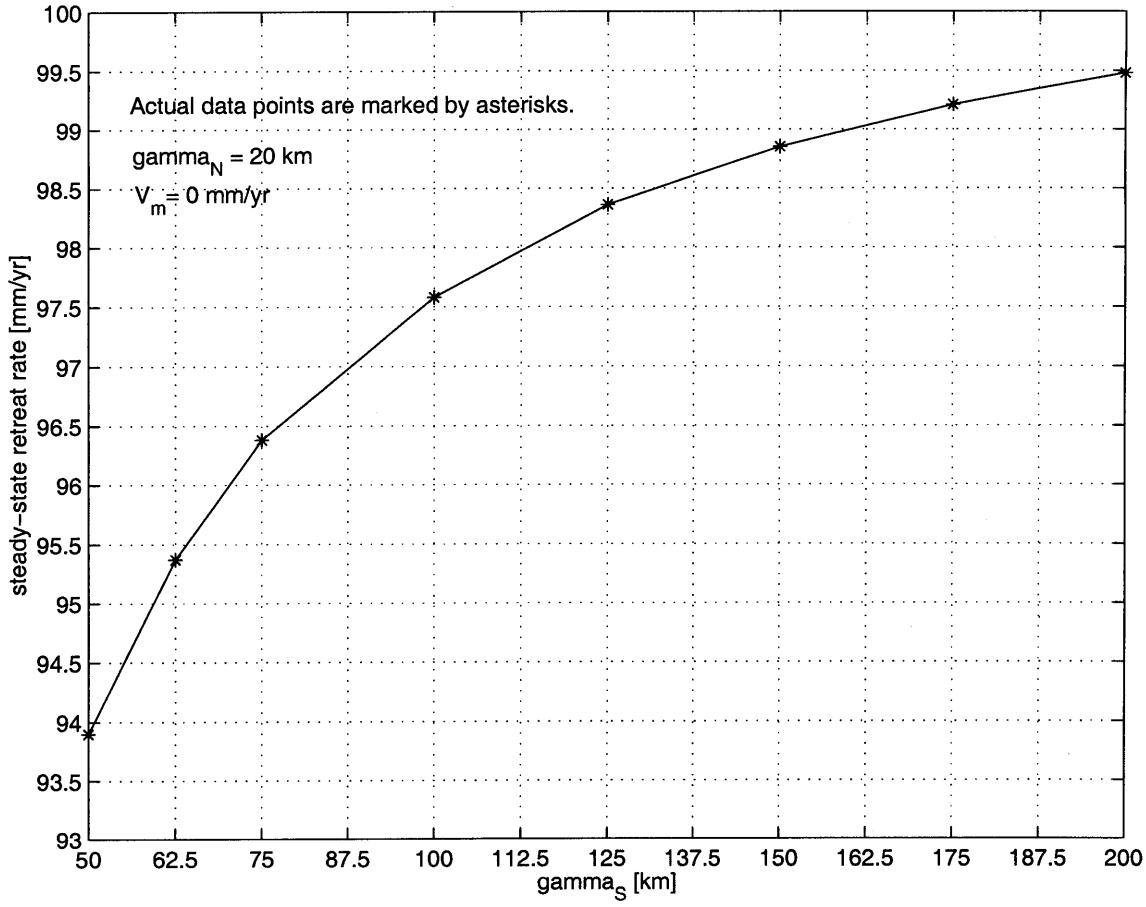

Figure A-12: Steady-state retreat rate plotted against γ_S (Stationary mantle)

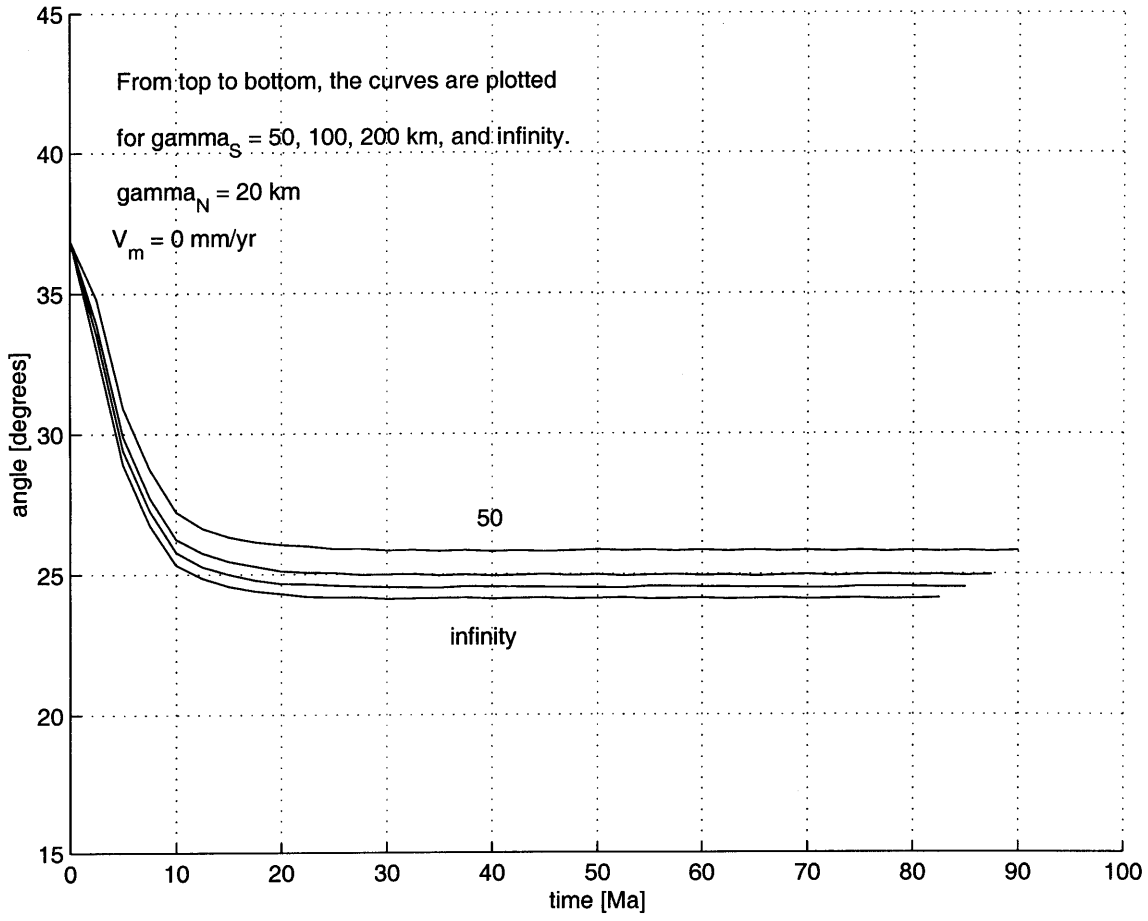

Figure A-13: Angle of subduction plotted against time (Stationary mantle)

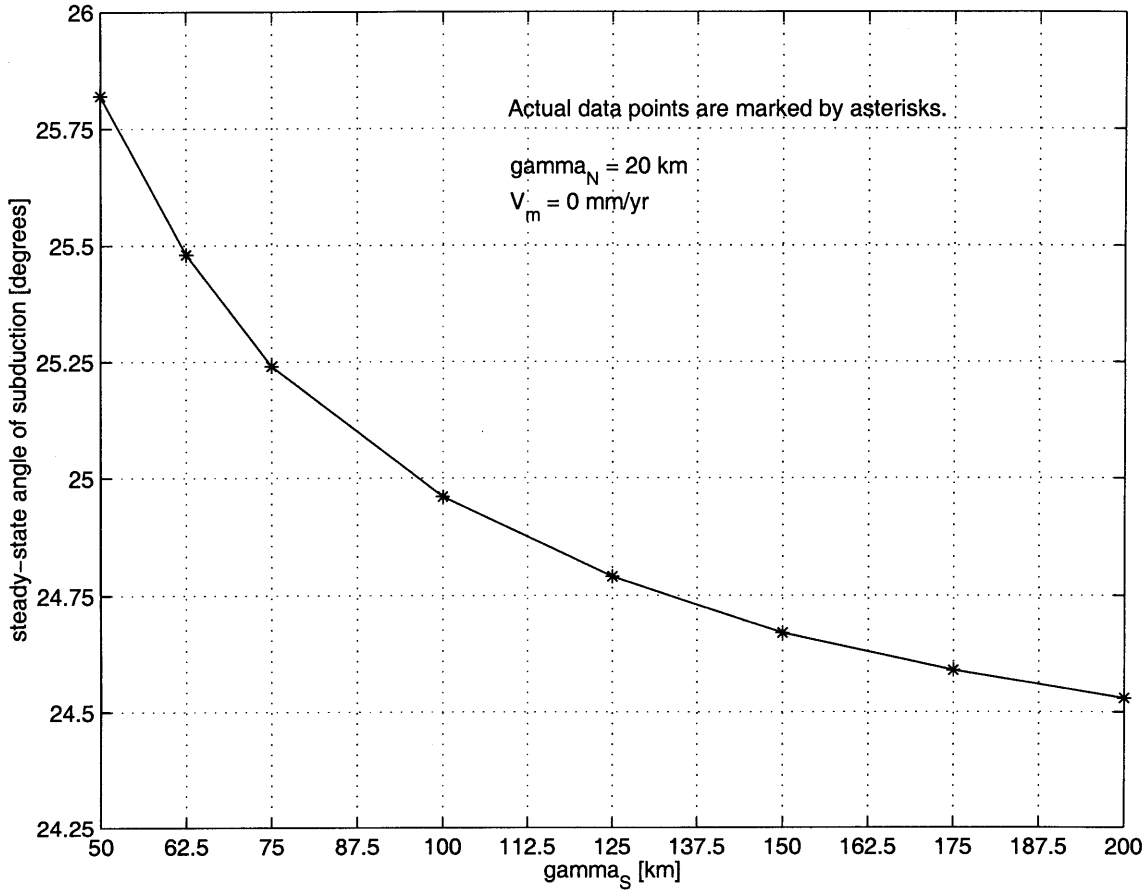

Figure A-14: Steady-state angle of subduction plotted against γ_S (Stationary mantle)

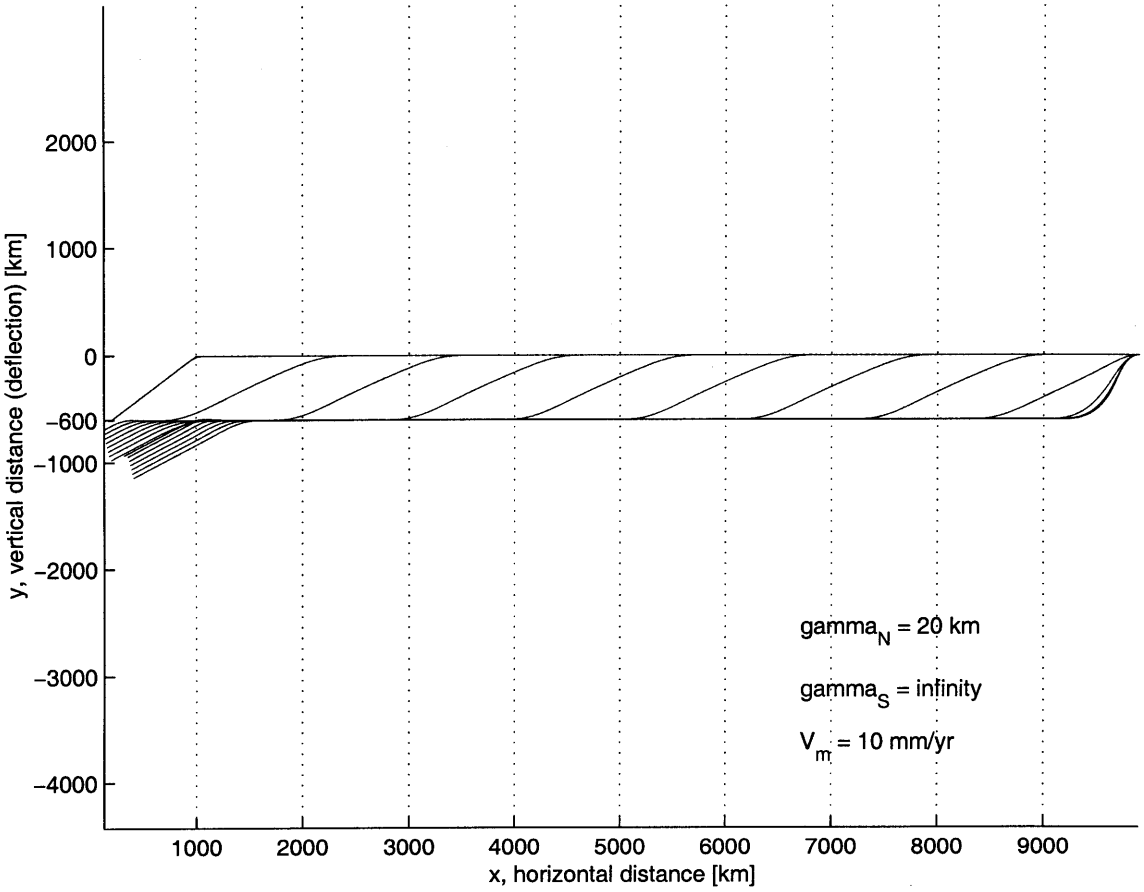

Figure A-15: Two-dimensional cross-sectional view of subduction (Stationary mantle). The slab does subduct deeper than 600km.

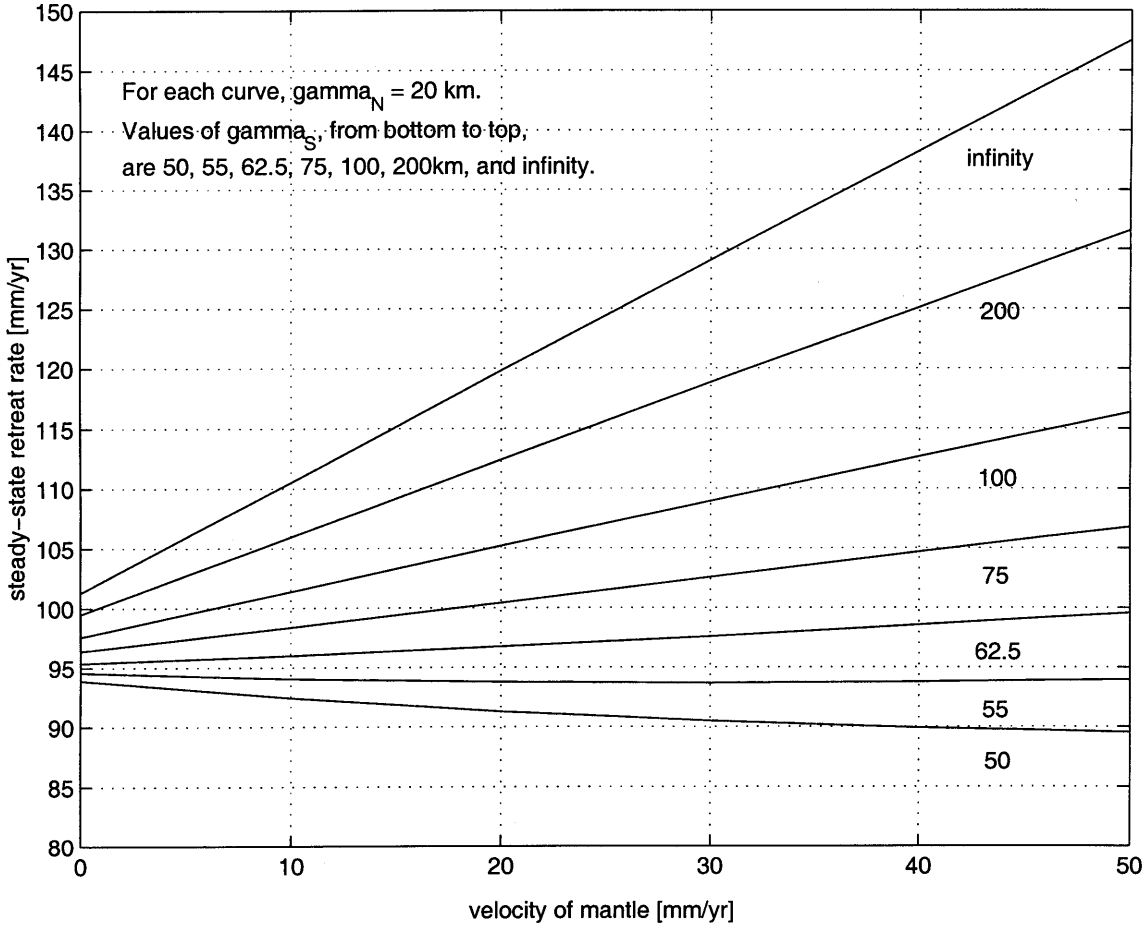

Figure A-16: Steady-state retreat rate plotted against the mantle velocity.

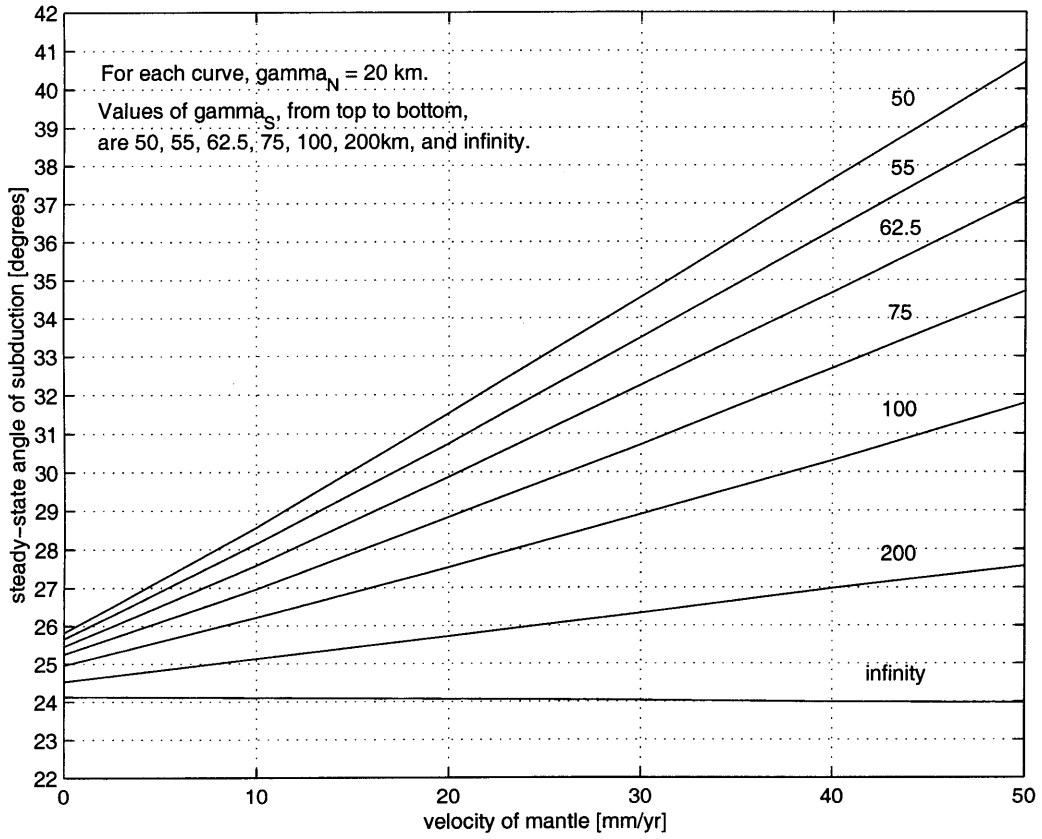

Figure A-17: Steady-state angle of subduction plotted against mantle velocity.

Appendix B

FORTRAN 90 Code

The code used for the numerical modeling discussed in this thesis is included in its entirety on the following pages.

```
************************************************************************
c234567890123456789012345678901234567890123456789012345678901234567890123456789012
c       1         2         3         4         5         6         7
************************************************************************
c     This FORTRAN 90 code uses a finite-difference approximation of
c     the flexure equation to compute the deflection of a subducting
c     slab through a series of time steps.
c
c     1/26/99 Wiki Royden began constructing this code
c     2/5/01  Matt Dawson began working with and adding to this code
c     4/26/01 Matt Dawson produces working version of this code
c     5/25/01 Matt Dawson edits code for inclusion in Master's Thesis
c     6/12/01 Matt Dawson completes Master's Thesis, inserts copy of
c             this code as Appendix B.

c     DEFINING PI (USED TO OUTPUT SUBDUCTION ANGLE)
      parameter(pi = 3.141592653589793)

c     define spatial arrays (input)
      real*8 dflex(1000),wo(1000),winit(1000)
      real*8 sflex(1000),so(1000),sinit(1000)

c     define temporal arrays (input)
      real*8 ucon(20)
      real*8 tcon(20)

c     define working arrays
      real*8 s(1000),win(1000),drig(1000),w(1000),xpos(1000)
      real*8 winteg(1000),wold(1000)
      real*8 ws(1000),wsq(1000)
```

```
c     DEFINE VELOCITY VARS.
c       (ONLY NEED THESE IN MAIN IF USED BY "output" SUBROUTINE)
c       VCON=Vasthenosphere. VNCON,VPCON=Va NORMAL, PARALLEL TO SLAB
c       VNL,VPL=Vel. OF SLAB IN DIRECTION NORMAL, PARALLEL TO SLAB
c       VC,HC=Vert., Horiz. COMPONENTS
      real*8 VCON
      real*8 VNL(1000),VNLVC(1000),VNLHC(1000)
      real*8 VPL(1000),VPLVC(1000),VPLHC(1000)
      real*8 VNCON(1000),VNCONVC(1000),VNCONHC(1000)                    40
      real*8 VPCON(1000),VPCONVC(1000),VPCONHC(1000)

c     DEFINE INPUT/OUTPUT FILES
c       in=input,out=output,prt=x-w data,rat=rate/angle data,ess=Spoints
      character*8 stem
      character*12 infile,outfile,prtfile,ratfile,essfile

 10   format(a8)

c     open input and output files                                       50
      write(*,*)'################################################'
      write(*,*)'name 8-letter file (eg. input file=filename.in)'
      read(*,10)stem
      infile = stem//'.in'
      outfile = stem//'.out'
      open(unit=3,file=infile,status='old')
      open(unit=7,file=outfile,status='unknown')
      prtfile = stem//'.prt'
      ratfile = stem//'.rat'
      open(unit=10,file=prtfile,status='unknown')                       60
```

```
      open(unit=11,file=ratfile,status='unknown')
      essfile = stem//'.ess'
      open(unit=15,file=essfile,status='unknown')

c     set initial values OF INPUT PARAMETERS
c     read PARAMS FROM INPUT FILES, CONVERT TO MKS, NON-DIMENSIONALI
      call input(dflex,sflex,wo,so,ucon,tcon,tottim,twrite,wmax
     1    ,delt,dels,amuo,icon,iflex,iwo,dref,wr,iend,gee,rhoc,rhoa
     2    ,dlen,dtim,dvel,dssq,ds4,iinit,sinit,winit,rhow,wlowman
     3    ,gamma,gammaN,gammaP,wcontest,wov,cov,alov,wovtest,rhom)      70

c     set up finite difference grid
      call setup(dflex,sflex,wo,so,dels,iflex,iwo,wr,iend
     1       ,s,win,drig,w,iinit,sinit,winit,wold,xpos
     2       ,xold,xxold,xxxold,wcontest,dlen,dvel,delt,dtim)

c     SET time COUNTERS TO 0.
      timtest=0.
      time=0.
      icount=0                                                        80

c     begin MAIN do loop here.  LOOP RUNS TO tottime AT STEPS OF delt
      do while (time.lt.tottim)
         time=time+delt
         timtest=timtest+delt

c     set VCON, Vastheno, FOR THIS TIME STEP
         do j=1,icon-1
            if (time.ge.tcon(j).and.time.lt.tcon(j+1)) VCON=ucon(j)
         end do                                                       90
```

```
c     SOLVE FLEXURE EQUATION TO find new values of deflection, w
      call nextw(iend,dels,delt,dssq,ds4,gamma,wr
     1     ,wmax,w,win,drig,xpos,s,rhoc,rhoa,rhow,wlowman
     2     ,rhom,cov,wov,alov,wovtest,dlen,wold
     3     ,time,dtim
     4     ,VCON,gammaN,gammaP,dvel,wcontest
     5     ,VNL,VNLVC,VNLHC,VPL,VPLVC,VPLHC
     6     ,VNCON,VNCONVC,VNCONHC,VPCON,VPCONVC,VPCONHC
     7     ,ws,wsq)                                                    100

c     INSTRUCT CODE TO OUTPUT RESULTS AFTER FIRST ITERATION
      if (time.eq.delt) then
         call output(iend,s,w,xpos,dlen,dvel,dtim,time
     1     ,drig,dref,win,wr,wmax,dels,told,wcontest
     2     ,VCON,VNCON,VNCONVC,VNCONHC,VPCON,VPCONVC,VPCONHC
     3     ,xmax,xmmax,xmmmax,xold,xxold,xxxold
     4     ,ws,wsq,pi)
      end if

                                                                       110
c     INSTRUCT CODE TO OUTPUT RESULTS
      if (timtest.ge.twrite) then
         timtest=timtest-twrite
         call output(iend,s,w,xpos,dlen,dvel,dtim,time
     1     ,drig,dref,win,wr,wmax,dels,told,wcontest
     2     ,VCON,VNCON,VNCONVC,VNCONHC,VPCON,VPCONVC,VPCONHC
     3     ,xmax,xmmax,xmmmax,xold,xxold,xxxold
     4     ,ws,wsq,pi)
      end if

                                                                       120
```

```
      icount=icount+1

c     end MAIN do loop here
      end do

 1001 format(i4,20(f15.8,1x))
 1002 format(500(f7.0,','))
 1000 format(500(f7.4,','))

      close(4)                                                    130
          stop
          end

*************************************************************************
c12345678901234567890123456789012345678901234567890123456789012345678901234567890123456789012
c        1         2         3         4         5         6         7
*************************************************************************

      subroutine input(dflex,sflex,wo,so,ucon,tcon,tottim,twrite,wmax    140
     1    ,delt,dels,amuo,icon,iflex,iwo,dref,wr,iend,gee,rhoc,rhoa
     2    ,dlen,dtim,dvel,dssq,ds4,iinit,sinit,winit,rhow,wlowman
     3    ,gamma,gammaN,gammaP,wcontest,wov,cov,alov,wovtest,rhom)

c     define spatial arrays
      real*8 dflex(1000),wo(1000),winit(1000)
      real*8 sflex(1000),so(1000),sinit(1000)

c     define temporal arrays (WE LET ucon [VCON] CHANGE W/ t)
      real*8 ucon(20)                                             150
```

```
      real*8 tcon(20)

c     tottim=total time (my)
c     twrite=time increment for output (my)
c     delt=time increment for calcs (my)

c     ucon="convergent rate", Vasthenosphere (mm/yr or km/my)
c     ucon [VCON] IS NEGATIVE TOWARD THE LEFT, POSITIVE TOWARD THE R
c     tcon=time control on "convergent rate" (mm/yr or km/my)
                                                                      160
c     dflex=flexural rigidity (Nm = kg m**2 /s**2))
c     sflex=position control on flexural rigidity (Nm = kg m**2 /s**2))
c     dref=reference flexural rigidity (Nm = kg m**2 /s**2))

c     dels = length increment along slab (km)

c     wo = initial water depth (km)
c     so = position control on initial water depth (km)
c     wr = water depth at mid-ocean ridge (km) (USED FOR ISOSTATIC BAL.)
c     wmax=max deflection with crust overlying at subduction boundary     170
c     wmax CONTROLS POSITION OF OVERRIDING CONTINENTAL PLATE
c     winit = intial deflection (INITIAL SLAB SHAPE)

c     amuo is reference viscosity OF ASTHENOSPHERE
c     gamma is length scale for mantle strain, USED TO ADJUST "VISCOSITY"
c     wcontest is depth INCREMENT USED TO TEST ROLLBACK RATES AND ANGL
c     "wcontest"=w (deflection)

c     gammaN is gamma in the Normal direction, ADJUSTS "NORMAL VISC"
c     gammaP is gamma in the Parallel direction, ADJUSTS "PARALLEL VISC"  180
```

```
      read(3,*)tottim,twrite,delt
c     units: my
      read(3,*)dels
c     units: km
      read(3,*)amuo, gamma, gammaN, gammaP
c     units: Pa s , km, km, km

c      READ Vasthenosphere
      do i=1,9999                                                    190
          read(3,*) icon,tcon(i),ucon(i)
c     units: INTEGER, Ma, km/Ma
          if (icon.eq.9999) go to 10
      end do
 10   icon=i

c      READ FLEXURAL RIGIDITY
      read(3,*) dref
c     units: Nm
                                                                     200
      do i=1,9999
          read(3,*) iflex,sflex(i),dflex(i)
c         units: INTEGER,km,Nm
          if (iflex.eq.9999) go to 20
      end do
 20   iflex=i

c      READ INITIAL WATER DEPTH & DENSITY PARAMETERS (OF UPPER PLA1
      read(3,*) wr,wmax,wcontest,wlowman
c     units: km,km,km,km                                             210
```

```
      read(3,*) wov,cov,alov,wovtest
c     units: km,km,km,km

c     READ MORE WATER DEPTH & DENSITY PARAMETERS (OF SUBDUCTING
      do i=1,9999
         read(3,*) iwo,so(i),wo(i)
c        units: km,km
         if (iwo.eq.9999) go to 30
      end do                                                    220
 30   iwo=i

c     READ INITIAL DEFLECTION (DEFINES INITIAL SHAPE OF SUBD. SLAB)
      do i=1,9999
         read(3,*) iinit,sinit(i),winit(i)
c        units: km,km
         if (iinit.eq.9999) go to 40
      end do
 40   iinit=i
                                                               230
c     set initial grid size (# OF NODES ALONG SUBDUCTING SLAB)
      read(3,*)iend

c     CONVERT all variables into MKS units
      tottim=tottim*(3.12e13)
      twrite=twrite*(3.12e13)
      delt=delt*(3.12e13)
      dels=dels*1000.

      do i=1,iflex                                              240
```

```
    sflex(i)=sflex(i)*1000.
end do

do i=1,icon
    ucon(i)=ucon(i)/(3.12e7)
    tcon(i)=tcon(i)*(3.12e13)
end do

wlowman=wlowman*1000.
wcontest=wcontest*1000.
wr=wr*1000.
wmax=wmax*1000.
wov=wov*1000.
cov=cov*1000.
alov=alov*1000.
wovtest=wovtest*1000.

gamma=gamma*1000.
gammaN=gammaN*1000.
gammaP=gammaP*1000.

do i=1,iwo
    so(i)=so(i)*1000.
    wo(i)=wo(i)*1000.
end do

do i=1,iinit
    sinit(i)=sinit(i)*1000.
    winit(i)=winit(i)*1000.
end do
```

```
c     DEFINE CONSTANTS FOR NON-DIM'N AND FLEXURE COMPUTATION
c       gee=GRAV. ACCEL., RHO_=DENSITY CRUST, ASTHENO, WATER, MANTLE
      gee=9.8
      rhoc=2700.
      rhoa=3200.
      rhow=1000.
c     make sure wov,cov,alov and rhom are compatible (BY ISOSTASY)
      rhom=((rhoa-rhow)*(wov-wr)-rhoc*cov+alov*rhoa)/(alov-cov)
                                                                    280
c     DEFINE FACTORS FOR NON-DIMENSIONALIZATION
      dlen=(dref/gee/(rhoa-rhow))**.25
      dtim=amuo/((rhoa-rhow)*gee*dlen)
      dvel=dlen/dtim

c     non-dimensionalize all variables
      tottim=tottim/dtim
      twrite=twrite/dtim
      delt=delt/dtim
      dels=dels/dlen                                                290

      do i=1,iflex
         sflex(i)=sflex(i)/dlen
         dflex(i)=dflex(i)/dref
      end do

      do i=1,icon
         ucon(i)=ucon(i)/dvel
         tcon(i)=tcon(i)/dtim
      end do                                                        300
```

```
      wlowman=wlowman/dlen

      wr=wr/dlen
      wcontest=wcontest/dlen
      wmax=wmax/dlen
      wov=wov/dlen
      cov=cov/dlen
      alov=alov/dlen
      wovtest=wovtest/dlen                                          310

      gamma=gamma/dlen
      gammaN=gammaN/dlen
      gammaP=gammaP/dlen

      do i=1,iwo
         so(i)=so(i)/dlen
         wo(i)=wo(i)/dlen
      end do
                                                                    320
      do i=1,iinit
         sinit(i)=sinit(i)/dlen
         winit(i)=winit(i)/dlen
      end do

c     reset dtim,dlen and dvel to YIELD UNITS OF Ma, mm/yr, km IN output
      dtim=dtim/(3.12e13)
      dvel=dvel*(3.12e7)*1000.
      dlen=dlen/1000.
                                                                    330
```

```
c     DEFINE SQUARE & 4th POWER OF ds FOR FINITE DIFF. APPROX.
      dssq=dels**2
      ds4=dels**4

      return
      end

**********************************************************************
c12345678901234567890123456789012345678901234567890123456789012345678901234567890
c       1         2         3         4         5         6         7          340
**********************************************************************

      subroutine setup(dflex,sflex,wo,so,dels,iflex,iwo,wr,iend
     1         ,s,win,drig,w,iinit,sinit,winit,wold,xpos
     2         ,xold,xxold,xxxold,wcontest,dlen,dvel,delt,dtim)

c     define spatial arrays
      real*8 dflex(1000),wo(1000),winit(1000)
      real*8 sflex(1000),so(1000),sinit(1000)
                                                                      350
      real*8 s(1000),win(1000),drig(1000),w(1000),winteg(1000)
      real*8 term1(1000),wold(1000),xpos(1000)

c     DEFINE wtotSETUP, IN ORDER TO PRINT INITIAL SLAB DEFLECTION DAT
      real*8 wtotSETUP

c       SETUP VECTOR FOR INITIAL DEFLECTION, w
        do i=1,iend
          s(i)=dels*float(i-1)
          do j=1,iinit-1                                              360
```

```
            if (s(i).ge.sinit(j).and.s(i).le.sinit(j+1))
     1          w(i)=winit(j) + (winit(j+1)-winit(j))
     2          *(s(i)-sinit(j))/(sinit(j+1)-sinit(j))
          end do
        end do

c       SETUP VECTOR FOR FLEXURAL RIGIDITY, D, OF SUBDUCTING SLAB
        do i=1,iend
          do j=1,iflex-1
            if (s(i).ge.sflex(j).and.s(i).le.sflex(j+1))                370
     1          drig(i)=dflex(j) + (dflex(j+1)-dflex(j))
     2          *(s(i)-sflex(j))/(sflex(j+1)-sflex(j))
          end do
        end do

c       SETUP VECTOR FOR "WATER DEPTH" (~DENSITY) OF SUBDUCTING SL.
c         NOTE: win IS ACTUALLY THE VERTICAL COMPONENT OF "Fgravity"
        do i=1,iend
          do j=1,iwo-1
            if (s(i).ge.so(j).and.s(i).le.so(j+1))                      380
     1          win(i)=(wo(j)-wr) + (wo(j+1)-wo(j))
     2          *(s(i)-so(j))/(so(j+1)-so(j))
          end do
        end do

c     find x-position, xpos, OF EACH NODE IN ORDER TO PLACE w
c       wstemp=TEMPORARY sine (ws) TERM, FORWARD DIFFERENCE
      xpos(iend)=s(iend)
      do i=iend-1,1,-1
        wstemp=(w(i+1)-w(i))/dels                                       390
```

```
      xpos(i)=xpos(i+1)-dels*sqrt(1.-wstemp**2)
     end do

c    INITIALIZED xold HERE SO IT HAS A VALUE WHEN 1st USED BY output
     do i=1,iend
          if (w(i).ge.wcontest.and.w(i+1).le.wcontest) then
            xold=xpos(i)+(wcontest-w(i))*(xpos(i+1)-xpos(i))
     1           /(w(i+1)-w(i))
          end if
          if (w(i).ge.wcontest*60. .and.w(i+1).le.wcontest*60.) then      400
            xxold=xpos(i)+(wcontest*60.-w(i))*(xpos(i+1)-xpos(i))
     1           /(w(i+1)-w(i))
          end if
         if (w(i).ge.wcontest*200. .and.w(i+1).le.wcontest*200.) then
            xxxold=xpos(i)+(wcontest*200.-w(i))*(xpos(i+1)-xpos(i))
     1           /(w(i+1)-w(i))
         end if
     end do

c    WRITE THESE INITIAL VALUES TO SCREEN (TO SEE IF THEY WORKED!)
     write(*,*)'XOLD1,XXOLD1,XXXOLD1 '
     1          ,xold*dlen,xxold*dlen,xxxold*dlen

c    WRITE INITIAL SHAPE TO FILES (t=0)
c      write deflection [DO LOOP]
c      wtotSETUP DEFINED INTERNALLY (IN setup SUBROUTINE), FOR EACH (i)
     do i=1,iend
c      FIND totAL DEFLECTION (IN setup SUBROUTINE) [AS IN output]
       wtotSETUP=w(i)+win(i)+wr
                                                                      420
```

```
c       WRITE x VS. w TO .out FILE (W/ & W/O DIMENSIONS)
        write(7,1200)xpos(i)*dlen,wtotSETUP*dlen,xpos(i),wtotSETUP

c       WRITE x VS. w TO .prt
        write(10,1201)xpos(i)*dlen,wtotSETUP*dlen

      end do
c     END WRITING DEFLECTION
c     END WRITING INITIAL SHAPE TO FILES (t=0)
                                                                      430
 1001 format(i4,20(f15.8,1x))
 1010 format(1x,50(f12.5,1x))
 1200 format(',',50(f8.2,',',f8.2,',     '))
 1201 format(1x,50(f12.5,1x))

        return
        end
*************************************************************************
c12345678901234567890123456789012345678901234567890123456789012345678901234567890123456789012
c       1       2       3       4       5       6       7               440
*************************************************************************
      subroutine nextw(iend,dels,delt,dssq,ds4,gamma,wr
     1     ,wmax,w,win,drig,xpos,s,rhoc,rhoa,rhow,wlowman
     2     ,rhom,cov,wov,alov,wovtest,dlen,wold
     3     ,time,dtim
     4     ,VCON,gammaN,gammaP,dvel,wcontest
     5     ,VNL,VNLVC,VNLHC,VPL,VPLVC,VPLHC
     6     ,VNCON,VNCONVC,VNCONHC,VPCON,VPCONVC,VPCONHC
     7     ,ws,wsq)
                                                                      450
```

```
c     computes w (DEFLECTION) AS f(s) (POSITION) for next time step

c     DEFINE dimension of incoming/outgoing variables
      real*8 w(1000),win(1000),drig(1000),xpos(1000)
      real*8 s(1000),winteg(1000),Dwsss(1000),wold(1000)
      real*8 vnvc(1000),vnhc(1000),Dwss(1000)

c     DEFINE dimension of internal variables
      real*8 ws(1000),wss(1000),term1(1000),wsq(1000)
      real*8 term(1000),aterm(1000),bterm(1000),dterm(1000)                460
      real*8 eterm(1000),fterm(1000),wintegold(1000),termww(1000)
      real*8 aaa(1000),bbb(1000),ccc(1000),ddd(1000),eee(1000)
      real*8 wint(1000),xint(1000),eps(1000),fvert(1000),fhori(1000)
      real*8 visc(1000),viscold(1000)

c     DEFINE DIMENSION OF VELOCITY-RELATED VARIABLES
      real*8 VCON
      real*8 VNL(1000),VNLVC(1000),VNLHC(1000)
      real*8 VPL(1000),VPLVC(1000),VPLHC(1000)
      real*8 VNCON(1000),VNCONVC(1000),VNCONHC(1000)                       470
      real*8 VPCON(1000),VPCONVC(1000),VPCONHC(1000)

c     DEFINE VARIABLES USED TO CALCULATE ABOVE VELOCITY COMPONEN
      real*8 Xlast(1000),Wlast(1000)
      real*8 deltaX(1000),deltaW(1000)
      real*8 deltaXN(1000),deltaWN(1000)
      real*8 deltaXP(1000),deltaWP(1000)

c     DEFINE VARIABLES USED TO "STRETCH" SLAB BACK TO INITIAL LENGT
      real*8 STRET(1000)                                                   480
```

```
      real*8 STRETw(1000),STRETx(1000)
      real*8 TOTSTRETw(1000),TOTSTRETx(1000)

c     DEFINE sine (ws) & cosine (wsq) TERMS, AS CENTERED DIFFERENCES (OG)
      do i=2,iend-1
            ws(i)=(w(i+1)-w(i-1))/dels/2.
            wsq(i)=sqrt(1.-ws(i)**2)
      end do
      ws(iend)=0.
      wsq(iend)=1.                                                    490
      ws(1)=ws(2)
      wsq(1)=wsq(2)

c     SET VISCOSITY STRUCTURE OF ASTHENO. (UNIFORM, INCREASE w/ DEP
      do i=1,iend
       visc(i)=1.
       viscold(i)=1.
       if (w(i).ge.wlowman) then
            visc(i)=1000.
            viscold(i)=1000.                                          500
       end if
       wold(i)=w(i)
      end do

c     BEGIN LOOP TO FIND 4th (dterm), 0th (bterm) and CONSTANT (eterm)
c      ORDER TERMS
      do i=1,iend

c     BTERM -> 0th ORDER TERM (EXTRACTED FROM q_n IN FLEXURE EQUATI
c      set modifiers for 'w' term in diff. (FLEXURE) eq.              510
```

```
      if (w(i).le.0.) then
        rhoinf=rhow
      else if (w(i)+win(i).le.cov+wov-wr) then
        rhoinf=rhoc
      else if (w(i)+win(i).le.alov+wov-wr) then
        rhoinf=rhom
      else
        rhoinf=rhoa
      end if
                                                                    520
c     CALCULATION OF bterm, ONLY INVOLVES Normal FORCES & VELOCITIES
      bterm(i)=(visc(i)/delt/gammaN)/sqrt(1.-ws(i)**2)
     1         +(rhoa-rhoinf)/(rhoa-rhow)

c     ETERM -> "CONSTANT" ORDER TERM (ALSO FROM q_n)
c      set modifiers for 'const' term in diff. (FLEXURE) eq.
c      fpcon = PRESSURE FROM "conTINENTAL" MATERIAL ABOVE SUBD. SLAB
c      fpcon DEPENDS ON POSITION OF SLAB-NODE BENEATH OVERRIDING PL
c      fpcon IS USED LATER FOR fvert & fhori OF 2nd ORDER TERM (aterm)
      if (w(i)+win(i).le.wmax+wov-wr) then                          530
        fpcon=-win(i)
      else if (w(i)+win(i).le.cov+wov-wr) then
        fpcon=(wr-wov)+(wov-wr-win(i))*(rhoa-rhoc)/(rhoa-rhow)
      else if (w(i)+win(i).le.alov+wov-wr) then
        fpcon=(wr-wov)+cov*(rhoc-rhom)/(rhoa-rhow)
     1         +(win(i)-(wov-wr))*(rhom-rhoa)/(rhoa-rhow)
      else
        fpcon=0.
      end if
                                                                    540
```

```
c     CALCULATION OF eterm, ONLY INVOLVES Normal FORCES & VELOCITIES
c      eterm = fpcon + Fgrav + Fvisc_Slabmotion + Fvisc_Asthenomotion
      eterm(i)=fpcon+win(i)*wsq(i)
     1   +(visc(i)*w(i)/delt/gammaN)/wsq(i)
     2   +(visc(i)*VNCON(i))/gammaN

c     DTERM -> 4th ORDER TERM     ( [D*wss]ss )
c        WATCH TO MAKE SURE wsq(i).ne.ZERO (THIS IS FIXED BY "STRETCH'
            dterm(i)=drig(i)/ds4/wsq(i)
                                                                      550
c     COMPUTE NET vert & horiz FORCES TO BE INTEGRATED IN 2nd ORDER TI
c     fvert= fpcon_vert + Fgrav_vert + P-due-to-deflection_vert
c     win(i)=Fgrav IN *VERTICAL* DIRECTION
      fvert(i)=fpcon*wsq(i)+win(i)
     1          -w(i)*wsq(i)*(rhoa-rhoinf)/(rhoa-rhow)
      fhori(i)=fpcon*(-ws(i))
     1          -w(i)*(-ws(i))*(rhoa-rhoinf)/(rhoa-rhow)

      end do
c     END DO LOOP FOR 4th, 0th, and "CONSTANT" ORDER TERMS   560

c     ATERM -> 2nd ORDER TERM ( wss*[Int_vert + Int_horiz] )
c     COMPUTE ADDITIONAL, VISCOUS INTEGRAL TERMS FOR 2nd ORDER TE
c     INITIALIZE INTEGRAL TERMS TO ZERO
      aint1=0.
      aint2=0.
      aint3=0.
      aint4=0.
      aint5=0.
      aint6=0.                                                        570
```

```
      aint7=0.
      aint8=0.
      aint9=0.
      aint10=0.

c     BEGIN aterm DO LOOP
c      VISCOUS FORCES=0  s=0 ( FREE SLAB END)
      aterm(1)=0.
c      NOW INTEGRATE ALONG THE PLATE FROM 2->s
      do i=2,iend                                                    580
        aint1=aint1+(fhori(i)+fhori(i-1))*dels/2.
        aint2=aint2+(fvert(i)+fvert(i-1))*dels/2.
        aint3=aint3+(VNLHC(i)+VNLHC(i-1))*dels/2.*viscold(i)/gammaN
        aint4=aint4+(VNLVC(i)+VNLVC(i-1))*dels/2.*viscold(i)/gammaN
        aint5=aint5+(VNCONHC(i)+VNCONHC(i-1))*dels/2.*viscold(i)/gammaN
        aint6=aint6+(VNCONVC(i)+VNCONVC(i-1))*dels/2.*viscold(i)/gammaN
        aint7=aint7+(VPCONHC(i)+VPCONHC(i-1))*dels/2.*viscold(i)/gammaP
        aint8=aint8+(VPCONVC(i)+VPCONVC(i-1))*dels/2.*viscold(i)/gammaP
        aint9=aint9+(VPLHC(i)+VPLHC(i-1))*dels/2.*viscold(i)/gammaP
        aint10=aint10+(VPLVC(i)+VPLVC(i-1))*dels/2.*viscold(i)/gammaP 590

c       SETS aint_=0 FOR w DEEPER THAN LOWER MANTLE (600km). WHY? ASK
c       (WHY NOT DO THE SAME FOR bterm?)
c       {IS THIS WHY SLAB GOES STRAIGHT IN LOWMANTLE? (wss=0)}
        if (w(i).ge.wlowman) then
          aint1=0.
          aint2=0.
          aint3=0.
          aint4=0.
          aint5=0.                                                   600
```

```
        aint6=0.
        aint7=0.
        aint8=0.
        aint9=0.
        aint10=0.
      end if

c     CALC. OF aterm, SUMMING INTEGRALS OF VT & HZ FORCE COMPONENTS
        aterm(i)=(aint1-aint3+ws(i)/wsq(i)*(aint2-aint4))/(dssq)
     1          +(aint5+ws(i)/wsq(i)*(aint6))/(dssq)                    610
     2          +(aint7+ws(i)/wsq(i)*(-aint8))/(dssq)
     3          +(aint9+ws(i)/wsq(i)*(-aint10))/(dssq)

      end do
c     END aterm DO LOOP (AND ATERM AS WELL)

c     NOW WE PREPARE TO SOLVE THE DIFF. EQ. FOR NEW w(i)
c      WE DO THIS BY SOLVING MATRIX EQ. Mx=y
c      1st SET UP FINITE DIFFERENCE MATRIX (M) FROM TERMS COMPUTED A
c      eterm, THE "CONSTANT" TERM WILL ACT AS "y" IN MATRIX EQ.  620
c     START W/ BOUNDARY CONDITIONS IN FIRST TWO ROWS, i=1,2
      do i=1,2
        eterm(i)=0.
        aaa(i)=0.
        bbb(i)=0.
        ccc(i)=1./dssq
        ddd(i)=-2./dssq
        eee(i)=1./dssq
      end do

                                                                        630
```

```
c     NOW FILL THE BULK OF THE MATRIX
      do i=3,iend-2
        aaa(i)=dterm(i-1)
        bbb(i)=-2.*dterm(i-1)-2.*dterm(i)+aterm(i)
        ccc(i)=dterm(i+1)+4.*dterm(i)+dterm(i-1)-2.*aterm(i)+bterm(i)
        ddd(i)=-2.*dterm(i+1)-2.*dterm(i)+aterm(i)
        eee(i)=dterm(i+1)
      end do

c     NOW FINISH MATRIX W/ B.CONDITIONS IN LAST 2 ROWS, i=(N-1),N 640
      do i=iend-1,iend
        eterm(i)=0.
        aaa(i)=0.
        bbb(i)=0.
        ccc(i)=1.
        ddd(i)=0.
        eee(i)=0.
      end do

c     *** NOW *PERFORM* THE MATRIX INVERSION W/ SPECIAL SUBROUTINE
      call inverse4(1,iend,eterm,wint,aaa,bbb,ccc,ddd,eee)

c     SAVE x,w VALUES FROM THE PREVIOUS TIME-STEP IN ORDER TO
c      COMPUTE THE VELOCITY OF THE SLAB AS IT MOVES TO A NEW POSIT.
      do i=1,iend
        Xlast(i)=xpos(i)
        Wlast(i)=w(i)
      end do

c     wint= w_intermediate, THE NEW DEFLECTION, FOUND BY INVERSE SUBROU
```

```
c     find x intermediate (xint) from w intermediate (wint) ...
c     ASSUMING EACH NODE OF THE SLAB MOVES
c     THEN "STRETCH" ... NOW FIND "NEW" dw & dx FOR VEL-COMPONENTS
      do i=1,iend
c       MOVE TO NEW w AT STEADY STATE ANGLE (works fine)
        xint(i)=Xlast(i)+(wint(i)-Wlast(i))*TAN(ASIN(-ws(i))/2.)
      end do

c     NEW x,w POSITIONS MAY BE INCOMPATIBLE WITH CONSTANT ds=10km
c     MUST STRETCH/SQUEEZE SLAB BACK TO ORIGINAL LENGTH TO CONTI
c     SLIDE EACH NODE ALONG SLAB UNTIL EACH ds=10km
      xint(iend)=s(iend)
      wint(iend)=wint(iend)

c     DETERMINE WHETHER EACH SEGMENT SHOULD BE STRETCHED OR SQU
c     THEN DETERMINE BY HOW MUCH
      do i=iend-1,1,-1
        STRET(i)=dels-sqrt(
     1       (wint(i)-wint(i+1))**2+(xint(i)-xint(i+1))**2 )
        if (xint(i)-xint(i+1).ne.0.) then                          680
c       IF SEGMENT IS VERTICAL, STRETx=0.
          STRETw(i)=STRET(i)*SIN(
     1       ATAN( ABS( (wint(i)-wint(i+1))/(xint(i)-xint(i+1)) ) )  )
          STRETx(i)=STRET(i)*COS(
     1       ATAN( ABS( (wint(i)-wint(i+1))/(xint(i)-xint(i+1)) ) )  )
        else
          STRETw(i)=STRET(i)
          STRETx(i)=0.
        end if
c       DETERMINE AND SET SIGN OF STRETCH/SQUEEZE                  690
```

```
      if (wint(i).lt.wint(i+1)) STRETw(i)=STRETw(i)*(-1.)
      if (xint(i).gt.xint(i+1)) STRETx(i)=STRETx(i)*(-1.)
    end do

c   "SUM-UP" TOTAL AMOUNT BY WHICH EACH *NODE* MUST BE TRANSLA
c    (LAST NODE,
    TOTSTRETw(iend)=0.
    TOTSTRETx(iend)=0.
    do i=iend-1,1,-1
c    SUM-UP TOTAL TRANSLATIONS WHILE MOVING DOWN THE PLATE TOW
      TOTSTRETw(i)=TOTSTRETw(i+1)+STRETw(i)
      TOTSTRETx(i)=TOTSTRETx(i+1)+STRETx(i)
    end do

c   TRANSLATE EACH NODE BY THE PROPER AMOUNT, FROM wint,xint-> w,x
    do i=iend,1,-1
      w(i)=wint(i)+TOTSTRETw(i)
      xpos(i)=xint(i)-TOTSTRETx(i)
    end do
                                                              710

c   CALCULATE ALL VELOCITY VECTORS
c    SIGNS MUST MATCH EVERYTHING ELSE, ESPECIALLY aterm
    do i=1,iend
c    deltaXN,deltaXP= CHANGE IN POSITION IN Normal OR Parallel DIR.
      deltaX(i)=(xpos(i)-Xlast(i))
      deltaW(i)=(w(i)-Wlast(i))
      deltaXN(i)=deltaX(i)*(-ws(i))
      deltaWN(i)=deltaW(i)*wsq(i)
c    FIND VELOCITY OF MOTION OF SUBDUCTING SLAB                720
```

```
      VNL(i)=(deltaXN(i)+deltaWN(i))/delt
      VNLVC(i)=VNL(i)*wsq(i)
      VNLHC(i)=VNL(i)*(-ws(i))
      deltaXP(i)=deltaX(i)*wsq(i)
      deltaWP(i)=deltaW(i)*(-ws(i))
      VPL(i)=(deltaWP(i)-deltaXP(i))/delt
      VPLVC(i)=VPL(i)*(-ws(i))
      VPLHC(i)=VPL(i)*wsq(i)
c     FIND VELOCITY OF Asthenosphere MOVING AGAINST SLAB (FROM VCON)
c       VNCON=VCON's Normal COMP. VNCON=VCON*sin(alpha).
      VNCON(i)=VCON*(-ws(i))
c     MIGHT WANT TO IGNORE Astheno MOTION WHERE SLAB IS HZ
c     if (w(i).lt.1.) VNCON(i)=0.
c       FIND VNCONHC=VNCON*sin(alpha) & VNCONVC=VNCON*cos(alpha)
      VNCONHC(i)=VNCON(i)*(-ws(i))
      VNCONVC(i)=VNCON(i)*wsq(i)
c       VPCON=VCON's Parallel COMP. VPCON=VCON*cos(alpha)
      VPCON(i)=VCON*wsq(i)
c     MIGHT WANT TO IGNORE Astheno MOTION WHERE SLAB IS HZ
c     if (w(i).lt.1.) VPCON(i)=0.
c       FIND VPCONHC=VPCON*cos(alpha) & VPCONVC=VPCON*sin(alpha)
      VPCONHC(i)=VPCON(i)*wsq(i)
c     VPCONVC(i)=VPCON(i)*(-ws(i))
c     VPCONVC should = VPCONHC.  try this to ensure that. (no matter)
      VPCONVC(i)=VNCONVC(i)
    end do

1001 format(i4,15(f12.6,1x))

    return
```

```
      end

*********************************************************************
c12345678901234567890123456789012345678901234567890123456789012345678901
c       1         2         3         4         5         6         7
*********************************************************************
      subroutine inverse4(ixbeg,ixend,y,x,A1,B1,C1,D1,E1)

c     SUBROUTINE INVERTS M, A NEARLY SYMMETRIC BAND MATRIX ...
c     WITH 5 NON-ZERO DIAGONALS                                      760
c     THE INVERSION EFFECTIVELY SOLVES Mx=y

c     M = FINITE DIFFERENCE MATRIX
c     x = UNKNOWN, NEW w TO BE FOUND, y = KNOWN "CONSTANT" TERM
c     z = DUMMY VAR = X + ONE OF THE SUB-MATRICES DECONVOLUTED FR
c     A1-E1 = BAND MATRIX COEFFICIENTS

c     assumes that the value of x at the grid ends is fixed at
c     y(ixbeg),y(ixend),y(ixbeg+1),y(ixend-1)
                                                                     770
c     DEFINE DIMENSION OF VARIABLES IN MATRIX EQUATION
      real*8 x(1000),y(1000),z(1000)
      real*8 A1(1000),B1(1000),C1(1000),D1(1000),E1(1000)
      real*8 a(1000),b(1000),c(1000),d(1000),e(1000)

c     TO EFFECTIVELY "INVERT" M ...
c     deconvolute matrix M into upper and lower band matrices
c     (a-c for lower matrix, 1,d,e for upper matrix)

c     perform matrix deconvolution                                   780
```

```
      i=ixbeg
            c(i)=C1(i)
            d(i)=D1(i)/c(i)
            e(i)=E1(i)/c(i)
      i=ixbeg+1
            b(i)=B1(i)
            c(i)=C1(i)-b(i)*d(i-1)
            d(i)=(D1(i)-b(i)*e(i-1))/c(i)
            e(i)=E1(i)/c(i)
      do i=ixbeg+2,ixend                                          790
            a(i)=A1(i)
            b(i)=B1(i)-a(i)*d(i-2)
            c(i)=C1(i)-a(i)*e(i-2)-b(i)*d(i-1)
            d(i)=(D1(i)-b(i)*e(i-1))/c(i)
            e(i)=E1(i)/c(i)
      end do

c     FIND VAR z BY "FORWARD SUBSTITUTION" WHERE z=y/(LOWER MATRIX
      i=ixbeg
         z(i)=y(i)/c(i)                                           800
      i=ixbeg+1
         z(i)=(y(i)-b(i)*z(i-1))/c(i)
      do i=ixbeg+2,ixend
         z(i)=(y(i)-b(i)*z(i-1)-a(i)*z(i-2))/c(i)
      end do

c     FIND X BY "BACK SUBSTITUTION" WHERE x = z/(UPPER MATRIX)
      i=ixend
         x(i)=z(i)
      i=ixend-1                                                   810
```

```
      x(i)=z(i)-d(i)*x(i+1)
    do i=ixend-2,ixbeg,-1
      x(i)=z(i)-d(i)*x(i+1)-e(i)*x(i+2)
    end do

c   NOW WE HAVE x(i), WHICH WILL RE-ENTER MAIN PROGRAM AS wint(i) ..
c   TO BE STRETCHED/SQUEEZED TO NEW w(i)

    return
      end                                                          820

*********************************************************************
c234567890123456789012345678901234567890123456789012345678901234567890123456789012
c       1         2         3         4         5         6         7
*********************************************************************
    subroutine output(iend,s,w,xpos,dlen,dvel,dtim,time
   1     ,drig,dref,win,wr,wmax,dels,told,wcontest
   2     ,VCON,VNCON,VNCONVC,VNCONHC,VPCON,VPCONVC,VPCONHC
   3     ,xmax,xmmax,xmmmax,xold,xxold,xxxold
   4     ,ws,wsq,pi)                                              830

c   SUBROUTINE PRINTS MODEL RESULTS TO FILES

c   DEFINE DIMENSION OF SPATIAL VARS (REQUIRED TO RECEIVE TRUE VA.
    real*8 s(1000),win(1000),drig(1000),w(1000),xpos(1000)
    real*8 ws(1000),wsq(1000)

c   DEFINE DIMENSION OF VELOCITY VARS (" ")
    real*8 VCON,VNCON(1000),VPCON(1000)
    real*8 VNCONVC(1000),VNCONHC(1000),VPCONVC(1000),VPCONHC(1000) 840
```

```
c     DEFINE INTERNAL VARIABLES (FOR SUBDUCTION ANGLE
      real*8 ANGLE300,ANGLE1000,ANGLE2000,ANGLE3000
      real*8 war(1000)

c     INITIALIZE THESE TO ZERO EACH TIME, TO "CLEAN" VAR.
      ANGLE300= 0.
      ANGLE1000=0.
      ANGLE2000=0.
      ANGLE3000=0.                                              850

c     WRITE TO SCREEN CURRENT Vasthenosphere, & PI
      write(*,*)' VCON=',VCON*dvel,'  PI=',pi

c     SET "wtot" (war) FOR RATE & ANGLE LOOP
      do i=1,iend
        war(i)=w(i)+win(i)+wr
      end do

c     WRITE time OF DATA TO BE PRINTED TO .out LATER            860
      write(7,*)' '
      write(7,*)'time (my) ',time*dtim

c     RATE & ANGLE LOOP
      do i=1,iend
c       compute convergence rate  (shallow)
c       note computed at deflection from initial (w)
c       not for absolute depth (w+win+wr)
c       FIND RATE
        if (w(i).ge.wcontest.and.w(i+1).le.wcontest) then       870
```

```
      xmax=xpos(i)+(wcontest-w(i))*(xpos(i+1)-xpos(i))
     1      /(w(i+1)-w(i))
      smax=s(i)+(wcontest-w(i))*(s(i+1)-s(i))
     2      /(w(i+1)-w(i))
      end if
c     FIND RATE & ANGLE ~300km  ( ABSOLUTE DEPTH)
      if (war(i).ge.wcontest*60. .and.war(i+1).le.wcontest*60.) then
       xmmax=xpos(i)+(wcontest*60.-war(i))*(xpos(i+1)-xpos(i))
     1      /(war(i+1)-war(i))
       smmax=s(i)+(wcontest*60.-war(i))*(s(i+1)-s(i))                    880
     2      /(war(i+1)-war(i))
       ANGLE300=(ASIN(-ws(i)))*(180/pi)
c      write(*,*)'ANGLE300 ',ANGLE300
      end if
c     FIND RATE & ANGLE ~1000 km DEPTH  ( ABSOLUTE DEPTH)
      if (war(i).ge.wcontest*200. .and.war(i+1).le.wcontest*200.) then
       xmmmax=xpos(i)+(wcontest*200.-war(i))*(xpos(i+1)-xpos(i))
     1      /(war(i+1)-war(i))
       smmmax=s(i)+(wcontest*200.-war(i))*(s(i+1)-s(i))
     2      /(war(i+1)-war(i))                                          890
       ANGLE1000=(ASIN(-ws(i)))*(180/pi)
       write(*,*)'ANGLE1000 ',ANGLE1000
      end if
c     FIND ANGLE ~2000km  ( ABSOLUTE DEPTH)
      if (war(i).ge.wcontest*400. .and.war(i+1).le.wcontest*400.) then
       ANGLE2000=(ASIN(-ws(i)))*(180/pi)
       write(*,*)'ANGLE2000 ',ANGLE2000
      end if
c     FIND ANGLE ~3000km  ( ABSOLUTE DEPTH)
      if (war(i).ge.wcontest*600. .and.war(i+1).le.wcontest*600.) then   900
```

```
        ANGLE3000=(ASIN(-ws(i)))*(180/pi)
        write(*,*)'ANGLE3000 ',ANGLE3000
      end if
    end do

    rate=(xmax-xold)/(time-told)
    ratedeeper=(xmmax-xxold)/(time-told)
    ratedeepest=(xmmmax-xxxold)/(time-told)

    write(*,*)'t=',time*dtim,'  rate,ratedeeper,xmax,xmmax '          910
   1     ,rate*dvel,ratedeeper*dvel,xmax*dlen,xmmax*dlen

c   WRITING t VS. rate AND ANGLE IN .rat FILE
    write(11,1009)time*dtim
   1              ,rate*dvel
   2              ,ratedeeper*dvel
   3              ,ANGLE300
   4              ,ANGLE1000

c   WRITE rate,xmax,xold TO .out FILE                                 920
    write(7,*)'conv rate, mm/yr, pos. new km, pos. old km ',
   1          rate*dlen/dtim,xmax*dlen,xold*dlen

c   ONLY WRITE DEFLECTION AT EVERY 10Ma INCREMENT
    if (MOD(NInt(time*dtim),10).eq.0) then

c   write deflection [DO LOOP]
c   wtot DEFINED INTERNALLY, FOR EACH (i)
    do i=1,iend
c     FIND totAL DEFLECTION, FIND SLOPE                               930
```

```
      wtot=w(i)+win(i)+wr
      slope=(w(i+1)-w(i))/(xpos(i+1)-xpos(i))

c     WRITE x VS. w TO .out FILE (W/ & W/O DIMENSIONS)
      write(7,1003)xpos(i)*dlen,wtot*dlen,xpos(i),wtot

c     WRITE x VS. w TO .prt
      write(10,1009)xpos(i)*dlen,wtot*dlen

c     PLOT DEFLECTION POINTS                                    940
      if (i.eq.299.or.i.eq.349.or.i.eq.399) then
        write(15,1009)xpos(i)*dlen,wtot*dlen
      end if

    end do
c   END WRITING DEFLECTION [DO LOOP]

    end if
c   END WRITING DEFLECTION [if]
                                                                950
c   RESET xold,told FOR NEXT RUN
    xold=xmax
    xxold=xmmax
    xxxold=xmmmax
    told=time

1001 format(i4,15(f12.5,1x))
1002 format(1x,6(f12.5,1x),3x,e10.3,3x,e10.3,2(f12.5))
1003 format(',',50(f8.2,',',f8.2,',     '))
1004 format(50(f6.0,','))                                       960
```

```
 1009 format(1x,50(f12.5,1x))
 1011 format(1x,50(f12.5,1x))
 1012 format(1x,50(f20.15,1x))
 1013 format(1x,50(f20.10,1x))

      return
      end

*******************************************************************************
c12345678901234567890123456789012345678901234567890123456789012345678901234567890 970
c       1       2       3       4       5       6       7
```

Bibliography

[1] M. Bevis. Geodetic observations of very rapid convergence and back-arc extension at the Tonga arc. *Nature*, 1995.

[2] C.M.R. Fowler. *THE SOLID EARTH An Introduction to Global Geophysics.* Cambridge University Press, Cambridge, 1990.

[3] X. Le Pichon and J. Angelier. The Hellenic arc and trench system: A key to the neotectonic evolution of the eastern Mediterranean area. *Tectonophysics*, 1979.

[4] J.E. Meulenkamp, M.J.R. Wortel, W.A. Van Wamel, W. Spakman, and E. Hoogerbuynstrating. On the Hellenic subduction zone and the geodynamic evolution of Crete since the late Middle Miocene. *Tectonophysics*, 1997.

[5] L.H. Royden. Evolution of retreating subduction boundaries formed during continental collision. *Tectonics*, 1993.

[6] L.H. Royden and F. Horvath. *The Pannonian Basin, a study in basin evolution.* American Association of Petroleum Geologists, 1988.

[7] Donald L. Turcotte and Gerald Schubert. *GEODYNAMICS Applications of Continuum Physics to Geological Problems.* John Wiley and Sons, New York, 1982.

[8] R.D. Van der Hilst, S. Widiyantoro, and E.R. Engdahl. Evidence for deep mantle circulation from global tomography. *Nature*, 1995.